High-Mannose Oligosaccharide Hemimimetics that Recapitulate the Conformation and Binding Mode to Concanavalin A, DC-SIGN and Langerin

Irene Herrera-González, Manuel González-cuesta, Michel Thépaut, Eugénie Laigre, David Goyard, Javier Rojo, José M García Fernández, Franck Fieschi, Olivier Renaudet, Pedro M Nieto, et al.

Chemistry Europe
European Chemical Societies Publishing

WILEY VCH

Excellence in Chemistry Research

Announcing our new flagship journal

- Gold Open Access
- Publishing charges waived
- Preprints welcome
- Edited by active scientists

Meet the Editors of *ChemistryEurope*

Luisa De Cola
Università degli Studi di Milano Statale, Italy

Ive Hermans
University of Wisconsin-Madison, USA

Ken Tanaka
Tokyo Institute of Technology, Japan

Chemistry–A European Journal
Research Article
doi.org/10.1002/chem.202303041
Chemistry Europe
European Chemical Societies Publishing
www.chemeurj.org

Hot Paper

High-Mannose Oligosaccharide Hemimimetics that Recapitulate the Conformation and Binding Mode to Concanavalin A, DC-SIGN and Langerin

Irene Herrera-González,[a, f] Manuel González-Cuesta,[a] Michel Thépaut,[b] Eugénie Laigre,[b, d] David Goyard,[d] Javier Rojo,[c] José M. García Fernández,[c] Franck Fieschi,[b, e] Olivier Renaudet,[d] Pedro M. Nieto,*[c] and Carmen Ortiz Mellet*[a]

The "carbohydrate chemical mimicry" exhibited by sp^2-iminosugars has been utilized to develop practical syntheses for analogs of the branched high-mannose-type oligosaccharides (HMOs) Man_3 and Man_5. In these compounds, the terminal nonreducing Man residues have been substituted with 5,6-oxomethylidenemannonojirimycin (OMJ) motifs. The resulting oligomannoside hemimimetic accurately reproduce the structure, configuration, and conformational behavior of the original mannooligosaccharides, as confirmed by NMR and computational techniques. Binding studies with mannose binding lectins, including concanavalin A, DC-SIGN, and langerin, by enzyme-linked lectin assay and surface plasmon resonance revealed significant variations in their ability to accommodate the OMJ unit in the mannose binding site. Intriguingly, OMJMan segments demonstrated "in line" heteromultivalent effects during binding to the three lectins. Similar to the mannobiose (Man_2) branches in HMOs, the binding modes involving the external or internal monosaccharide unit at the carbohydrate binding-domain exist in equilibrium, facilitating sliding and recapture processes. This equilibrium, which influences the multivalent binding of HMOs, can be finely modulated upon incorporation of the OMJ sp^2-iminosugar caps. As a proof of concept, the affinity and selectivity towards DC-SIGN and langerin were adjustable by presenting the OMJMan epitope in platforms with diverse architectures and valencies.

Introduction

Calcium(II)-dependent lectin receptors (CLRs) play a crucial role in the innate immune response by exhibiting specificity towards high mannose oligosaccharides (HMOs) and mannose-containing polysaccharides.[1] They contribute to various functions, including driving immune cell migration to sites of inflammation or peripheral lymphatic nodes, as well as facilitating the endocytosis and digestion of potentially harmful pathogens.[2] Notable examples of this category of carbohydrate-binding proteins include the macrophage receptor (MR), mannose binding lectin (MBL), dectin-2, langerin, and dendritic cell-specific intercellular adhesion molecule 3-grabbing nonintegrin (DC-SIGN).[3]

These CLRs display a common group of amino acids at the Ca^{2+} coordination site of the carbohydrate recognition domain (CRD).[4] Although they exhibit dissimilarities in the adjacent sequences of the CRD, leading to distinct secondary binding site profiles, they share affinity towards a broad range of natural and synthetic glycoligands. However, the downstream events upon binding can vary significantly. As an illustrative example, the binding of high mannose oligosaccharides (HMOs) on the surface of the human immunodeficiency virus (HIV) by DC-SIGN expressed in dendritic cells (DCs) results in immune system hijacking and facilitates virus propagation.[5] Conversely, binding to langerin in Langerhans cells (LCs) leads to HIV encapsulation, effectively halting the infection process.[6] These distinct outcomes highlight the significant functional implications of selective recognition of mannose-binding CLRs. Unsurprisingly,

[a] Dr. I. Herrera-González, Dr. M. González-Cuesta, Prof. C. Ortiz Mellet
Department of Organic Chemistry, Faculty of Chemistry
University of Seville
C/ Profesor García González 1, 41012 Sevilla (Spain)
E-mail: mellet@us.es
[b] Dr. M. Thépaut, Dr. E. Laigre, Prof. F. Fieschi
Institut de Biologie Structurale
Université Grenoble Alpes, CNRS, CEA
38000 Grenoble (France)
[c] Dr. J. Rojo, Dr. J. M. García Fernández, Dr. P. M. Nieto
Instituto de Investigaciones Químicas (IIQ)
CSIC – Universidad de Sevilla
Américo Vespucio 49, 41092 Sevilla (Spain)
E-mail: pedro.nieto@iiq.csic.es
[d] Dr. E. Laigre, Dr. D. Goyard, Prof. O. Renaudet
DCM, UMR 5250
Université Grenoble Alpes, CNRS
570 Rue de la Chimie, 38000 Grenoble (France)
[e] Prof. F. Fieschi
Institut Universitaire de France (IUF)
Paris (France)
[f] Dr. I. Herrera-González
Present address:
DCM, UMR 5250
Université Grenoble Alpes, CNRS
570 Rue de la Chimie, 38000 Grenoble (France)

Supporting information for this article is available on the WWW under https://doi.org/10.1002/chem.202303041

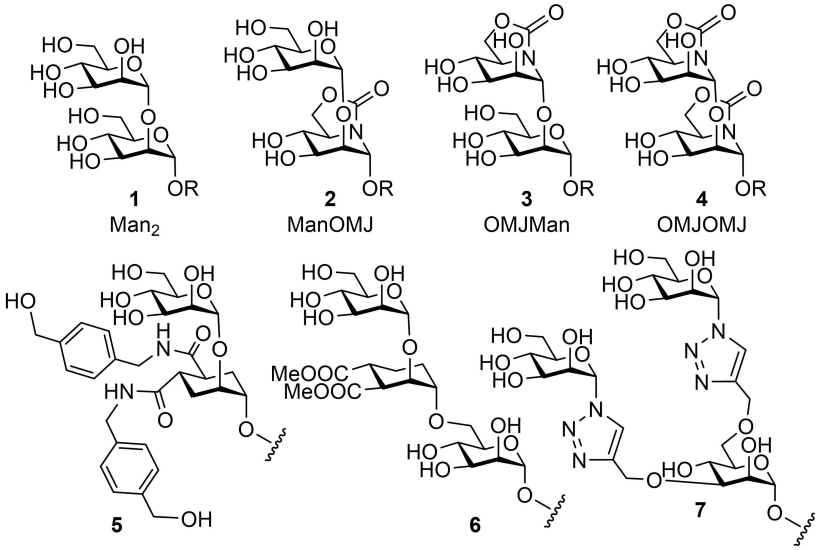

Figure 1. Structures of mannobiose (**1**) and 5,6-oxomethylidenemannonojirimycin (OMJ)-based mannobiose mimetics (**2**–**4**). Examples of cyclohexane- (**5**, **6**) or 1,2,3,–triazole-based (pseudo)mannooligosaccharide (**7**) derivatives are also shown. R represents 2-azidoethyl (for **2**–**4**) or Me (for **1**).

this has long been a sought-after goal in glycobiology, both for advancing fundamental studies on the immunomodulatory functions of these receptors and developing novel therapies.[7,8]

A compelling body of evidence supports α(1,2)-linked mannobiose (Manα(1,2)Man, Man_2, **1**; Figure 1) as a preferred glycotope for mannose-specific CLRs.[9] Unlike other positional isomers of mannodisaccharides, both the reducing and non-reducing mannose units in Man_2 can bind to the CRD in the corresponding complex.[10] This unique behavior was initially observed in the binding of Man_2 to the plant lectin concanavalin A (ConA)[11] and represents the simplest case of a divalent "in-line"[12] glycoligand/lectin interaction. The recognition event benefits from typical multivalent mechanisms, such as sliding and rebinding phenomena, resulting in significantly higher affinities than expected from a simple statistical effect.[13]

Man_2 is considered a heterodivalent compound since the two mannose constituents are not equivalent. When encountering a lectin partner, subtle differences in preference for one pose over the other may arise depending on the CRD architecture. In a preliminary communication, we suggested that such differences could be amplified when using Manα(1,2)Man mimetics where one or both of the monosaccharide moieties are replaced by a sp^2-iminosugar-type glycomimetic.[14] sp^2-Iminosugars are monosaccharide surrogates that, formally, replace the characteristic endocyclic oxygen with a pseudoamide-type nitrogen atom exhibiting substantial sp^2-hybridization.[15] Unlike classical iminosugars, sp^2-iminosugars can participate in glycosylation reactions, yielding chemically stable α-glycoside-like derivatives due to an enhanced anomeric effect.[16] Therefore, we synthesized compounds **2**–**4**, which comprise 5,6-oxomethylidenemannonojirimycin (OMJ) motifs, featuring a configurational pattern identical to that of α-D-mannopyranosides (Figure 2).[17] Encouragingly, ligands with complete discrimination capabilities towards DC-SIGN compared to langerin

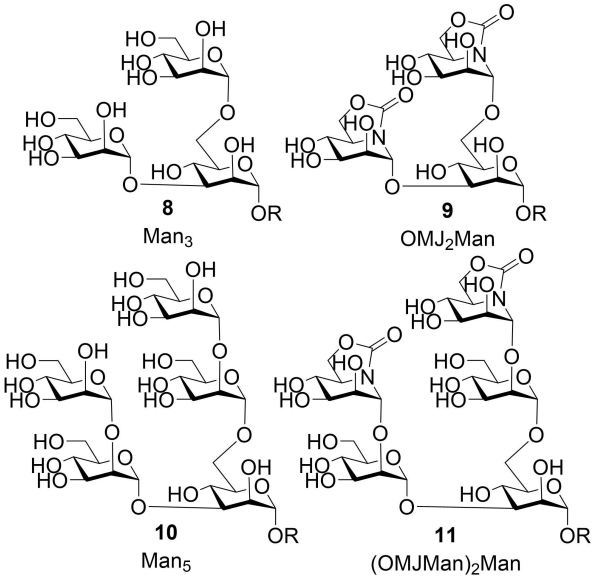

Figure 2. Structures of the (pseudo)mannooligosaccharides **8**–**11**. R represents 2-azidoethyl.

were engineered by presenting the pseudodisaccharide OMJα(1,2)Man (OMJMan, **3**) in multiple copies on a β-cyclodextrin (βCD) platform.[14,18]

In principle, higher analogs of HMOs incorporating both mannose and OMJ units (referred to as HMO hemimimetics) can be synthesized by replicating the established procedures used for the parent oligosaccharides. In contrast to the utilization of cyclohexane[19] or 1,2,3-triazole platforms[20] as mannose mimetics for emulating Man units in Man_2 and HMO-related mannooligosaccharides (e.g., **5**–**7**; Figure 1), the OMJ sp^2-iminosugar accurately reproduces the substitution arrangement of α-mannopyranosyl residues. We hypothesized that the presence of different OMJ moieties in the structure would have

varying effects on the recognition of mannose-binding lectins within a series. (Hetero)multivalent effects, which are highly sensitive to ligand density and topological characteristics,[21] are anticipated to further contribute to lectin discernment when multiconjugation is employed, providing an additional level of customization. By combining the functional toolbox of HMO mimics based on sp^2-iminosugars with appropriate scaffolds, the opportunities for selective targeting of CLRs can be significantly expanded. To explore these concepts, we have conducted a comprehensive investigation encompassing synthetic, spectroscopic, computational, and biophysical studies. Specifically, our objectives were as follows:

(a) Expansion of the sp^2-iminosugar-based HMO mimetics from Man_2 to include analogs of the branched mannooligosaccharide glycosides Man_3 (**8**) and Man_5 (**10**), namely compounds OMJ_2Man (**9**) and $(OMJMan)_2Man$ (**11**), respectively (Figure 2).

(b) Profiling the conformational properties and recognition abilities of the entire series of (pseudo)HMOs against the model lectin ConA and the human CLRs DC-SIGN and langerin.

(c) Preparation of a diverse range of conjugates displaying the preferred mannobiose hemimimetic motif OMJMan on various platforms with different valencies, densities, and architectures, to enable probing assays for investigating lectin recognition variations.

Results and Discussion

Synthesis and conformational properties of sp^2-iminosugar-terminated mannooligosaccharide hemimimetics

After identifying OMJMan as a privileged motif for selective targeting of DC-SIGN, our synthetic efforts have been focused on preparing hemimimetics of higher HMOs with terminal (non-reducing) OMJ units. To maintain sequence homology, we installed an α-oriented 2-azidoethyl aglycone. The synthesis of the pseudotrisaccharide OMJ_2Man glycoside **9** was achieved by reacting the Man dual acceptor **12**[22] with the OMJ pseudoglycosyl fluoride **13**[23] (→**14**, 71%) and subsequently catalytically removing the ester protecting groups (Scheme 1). A convergent strategy was employed for the synthesis of the pseudopentasaccharide $(OMJMan)_2Man$ glycoside **11**, which involved the same monosaccharide acceptor **12** and the protected OMJMan pseudodisaccharide trichloroacetimidate **17** as the glycosyl donor (→**18**, 50%), followed by deacylation (Scheme 2). Compound **17** was synthesized in three steps starting from the Man tolylthioglycoside tribenzoate **15** [24], which included glycosylation with **13** (→**16**, 64%), removal of the *S*-tolyl group using N-bromosuccinimide (NBS), and reaction of the crude reducing intermediate with trichloroacetonitrile/1,8-diazabicyclo[5.4.0]undec-7-ene (DBU; 34%). Equivalent synthetic routes were used to access the corresponding 2-azidoethyl Man_3[25] and Man_5[26] α-glycosides, which were employed as controls in structural and lectin recognition experiments. These results exemplify the versatility of sp^2-iminosugars in integrating standard glycosidation methodologies, underscoring their unique "carbohydrate chemical mimic" properties.

The ability of OMJ-containing mannooligosaccharides to replicate the conformational behavior of the parent glycans was initially assessed through Monte Carlo Multiple Minimum (MCMM)[27,28] conformational searches followed by Monte Carlo/Stochastic Dynamics (MC/SD)[29] simulations at 300 K using the OPLS3e force field implemented in Maestro 12.2 (MacroModel 12.6) software.[30] To validate the method, we first examined methyl α-(1,2)-mannobioside (Man_2OMe; **1**-OMe). Previously reported NMR and computational data for Man_2OMe in water indicated an equilibrium between a stacked (*S*) and an extended (*E*) conformation around the glycosidic linkage, with both conformations being similarly populated.[31,32] The *S* conformation is characterized by ϕ (H1′-C1′-O1′-C2) and ψ (C1′-O1′-C2-H2) dihedral angle values ranging from −30° to +30° and +30° to +50°, respectively, consistent with H-1/H-1′ NOE contacts (Supporting Information, Figure S49). The less flexible *E* conformation exhibits ϕ and ψ values around −50° and −30° to +30°, respectively, in agreement with H-5′/H-1 and H-1′/H-3 diagnostic NOE signals. We successfully reproduced this scenario (refer to the Supplementary Information for computational details).

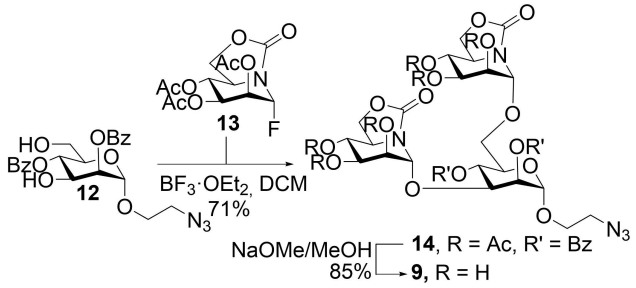

Scheme 1. Synthesis of the OMJ_2Man glycoside **9**.

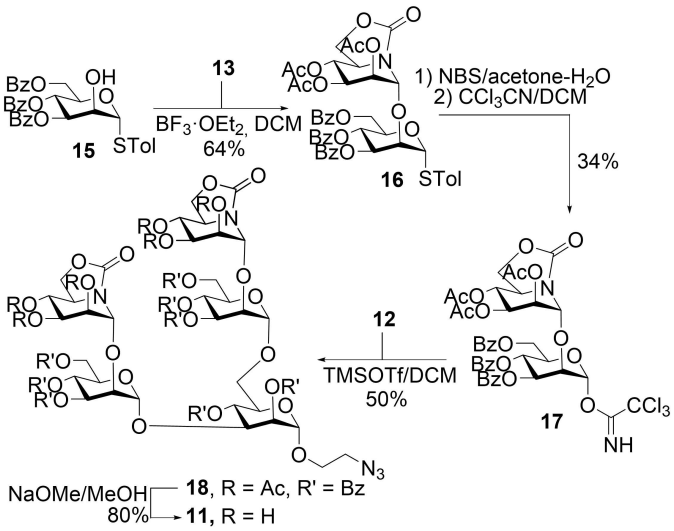

Scheme 2. Synthesis of the $(OMJMan)_2Man$ glycoside **11**.

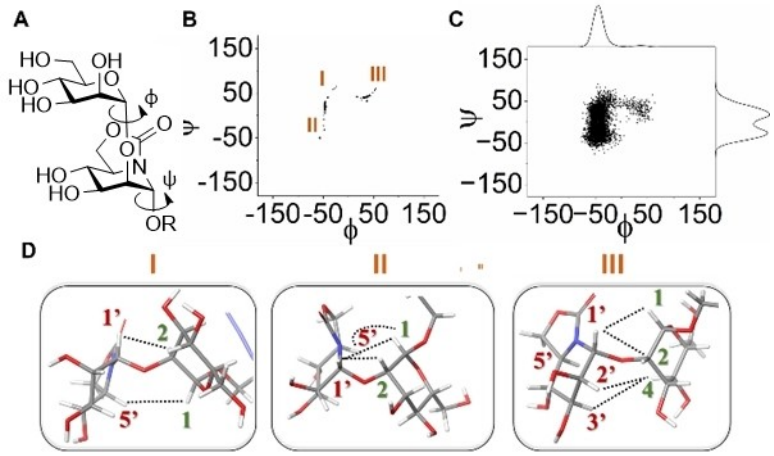

Figure 3. A) Structure of the OMJMan pseudodisaccharide **3** with indication of the ϕ (H1′-C1′-O1′-C2) and ψ (C1′-O1′-C2-H2) dihedral angles defined for computational experiments. B) (ϕ,ψ) map obtained by the conformational search (MCMM/OPL3e force field). C) (ϕ,ψ) map obtained after MC/SD simulation. D) Representation of the minimum energy conformations for regions I, II and III in the (ϕ,ψ) map, with indication of the theoretical diagnostic NOE contacts.

We subsequently applied the validated molecular modeling protocol in combination with NMR spectroscopy to investigate the conformational properties of the sp^2-iminosugar-based Man_2 mimetics **2**–**4** previously synthesized. The MCMM-generated (ϕ,ψ) maps exhibited similar patterns for all the pseudodisaccharides. In this discussion, we will focus on the conformational analysis of the OMJMan glycoside **3** as an illustrative case (Figure 3A), while the complete dataset is provided in the Supplementary Information (Supporting Information, Figures S50–S57 and Tables S1 and S2). Three regions (I–III) with relative energies below 20 kJ mol^{-1} were identified (Figure 3B). Region I, representing the energy minimum, and region II (+2.4 kJ mol^{-1}) correspond to *E*-conformers and possess (ϕ,ψ) values of approximately (−47°,+17°) and (−49°,−34°), respectively. Region III (+2.4 kJ mol^{-1}) contains *S*-conformers with (ϕ,ψ) values of about (+26°,+18°). Molecular dynamics simulations at 300 K for a duration of 10 ns supported a rapid conformational equilibrium around the glycosidic linkage and revealed a greater tendency to occupy *E*-conformer regions compared to Man_2OMe (Figure 3C). The predicted proton-proton contacts from the MCMM analysis (Figure 3D) were corroborated by NOE experiments (Supporting Information, Figures S53 and S54), which also provided experimental interproton distances that matched well with the distances calculated through MC/SD (Table 1). Comparison of such distance with the corresponding interproton distance range reported for the mannobioside **1**-OMe further confirmed the prevalence of the *E* conformation.

Table 1. Theoretical (MC/SD) and experimental distances (NOESY) for diagnostic interproton distances (*d*) for the OMJMan glycoside **3**. The reported experimental distance range for the methyl mannobioside **1**-OMe are also shown for comparative purposes.

Proton pair	$d_{MC/SD}$ [Å]	d_{Exp} [Å]	d_{Exp} for 1-OMe [Å]
H-1′/H-1	3.39	3.46	2.9–3.0
H-1′/H-2	2.38	2.41	2.1–2.2
H-5′/H-1	2.49	2.59	2.5–2.7

For the Man_3 surrogate OMJ_2Man glycoside **9**, which contains two glycosidic linkages, namely α(1,3) and α(1,6), we defined the following dihedral angles (Figure 4A): $\phi_{C,A}$ ($N5^C$-$C1^C$-$O3^A$-$C3^A$), $\psi_{C,A}$ ($C1^C$-$O3^A$-$C3^A$-$C2^A$), $\phi_{B,A}$ ($N5^B$-$C1^B$-$O6^A$-$C6^A$), $\psi_{B,A}$ ($C1^B$-$O6^A$-$C6^A$-$C5^A$), and $\omega_{B,A}$ ($O6^A$-$C6^A$-$C5^A$-$C4^A$). MCMM conformational searches were performed to generate ($\phi_{C,A}$,$\psi_{C,A}$) and ($\phi_{B,A}$,$\psi_{B,A}$) maps, which revealed three regions (I–III and IV–VI, respectively; Figure 4B) with relative energies below 20 kJ mol^{-1}. To facilitate comparison, the maps for each glycosidic linkage are presented in Figure 4 alongside the corresponding maps obtained for the parent Man_3 glycoside **8** in a parallel analysis (Figure 4C). Region I represents the energy minimum for the α(1,3) linkage at ($\phi_{C,A}$,$\psi_{C,A}$)=(−46°,+13°). Rotation around $\psi_{C,A}$ leads to region II (+1.2 kJ mol^{-1}), while region III is obtained by rotating around $\phi_{C,A}$ to approximately +30° (+9.6 kJ mol^{-1}). In addition to the typical through-space coupling between the protons on the carbons directly involved in the glycosidic connection ($H1^C$ and $H3^A$), conformers located in region III are expected to exhibit a NOE contact between $H1^C$ and $H2^A$, which was experimentally observed for both OMJ_2Man (Figure 4D) and Man_3. The α(1,6) glycosidic linkage is predicted to be more flexible. In contrast to the relatively confined regions I–III observed in the ($\phi_{C,A}$,$\psi_{C,A}$) map, regions IV–VI in the ($\phi_{B,A}$,$\psi_{B,A}$) map of OMJ_2Man showed a wider distribution of the $\psi_{B,A}$ angle compared to the natural mannotrisaccharide Man_3 (Figure 4B and C). However, the MC/SD simulations provided similar overall conformational tendencies. The $\phi_{C,A}$ and $\phi_{B,A}$ angles remained close to −50° for the majority of the simulation time, and the α(1,3) and α(1,6) linkages predominantly adopted conformations within regions I, II, and IV, V, respectively. A minor population of non-exoanomeric conformations, characterized by positive values of ϕ and ψ, was also observed for both glycosidic linkages (Figure 4E and F).

The torsion angle around C5-C6 predominantly adopted two conformations (Figure 5A and B): *gauche-trans* (*gt*; $\omega_{B,A}=\pm$

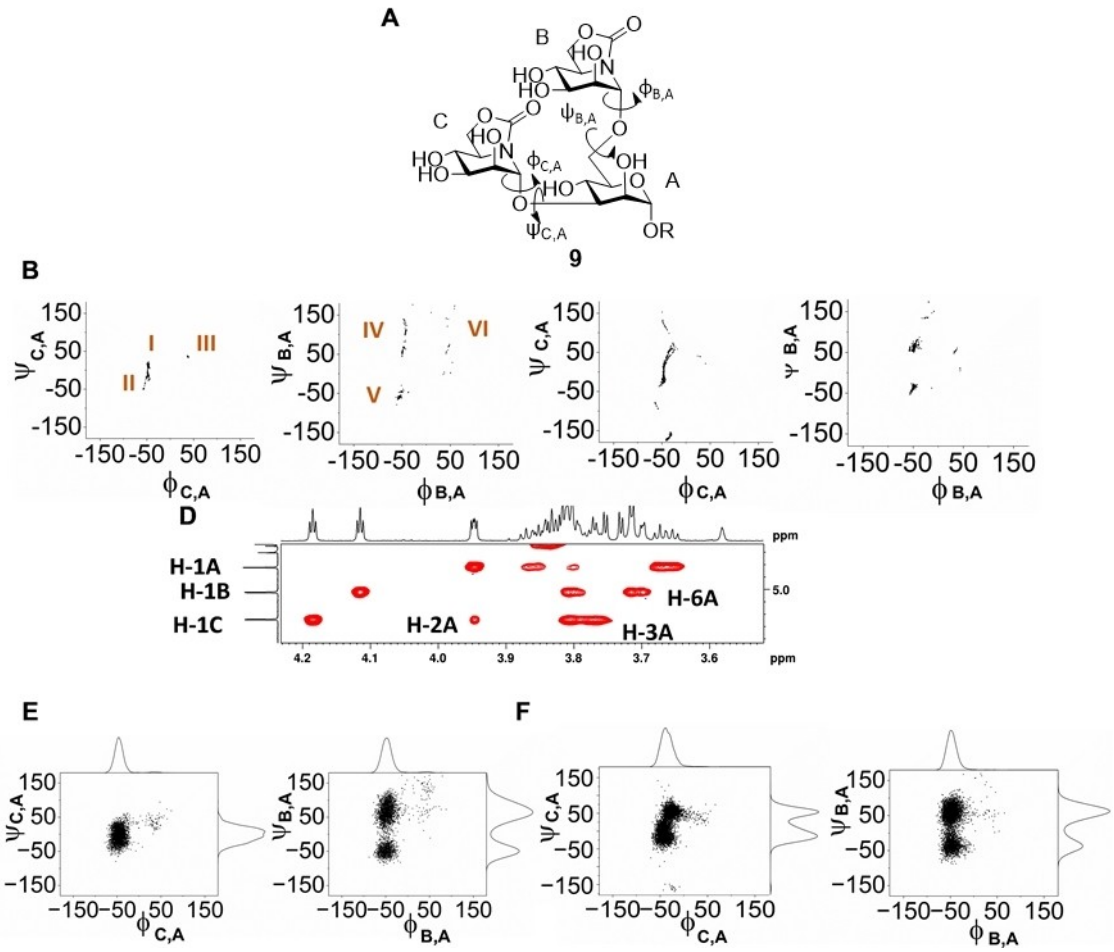

Figure 4. A) Structure of the OMJ_2Man glycoside **9** with indication of the $\phi_{C,A}$ ($N5^C$-$C1^C$-$O3^A$-$C3^A$), $\psi_{C,A}$ ($C1^C$-$O3^A$-$C3^A$-$C2^A$), $\phi_{B,A}$ ($N5^B$-$C1^B$-$O6^A$-$C6^A$), $\psi_{B,A}$ ($C1^B$-$O6^A$-$C6^A$-$C5^A$), and $\omega_{B,A}$ ($O6^A$-$C6^A$-$C5^A$-$C4^A$) dihedral angles defined for computational experiments. B and C) (ϕ,ψ) maps obtained by the conformational search (MCMM/OPL3e force field) for the OMJ_2Man and Man_3 (pseudo)glycosides **9** and **8**, respectively. D) Expansion of the NOESY spectrum for the OMJ_2Man glycoside **9**. E and F) (ϕ,ψ) maps obtained by MC/SD simulation for the OMJ_2Man and Man_3 (pseudo)glycosides **9** and **8**, respectively.

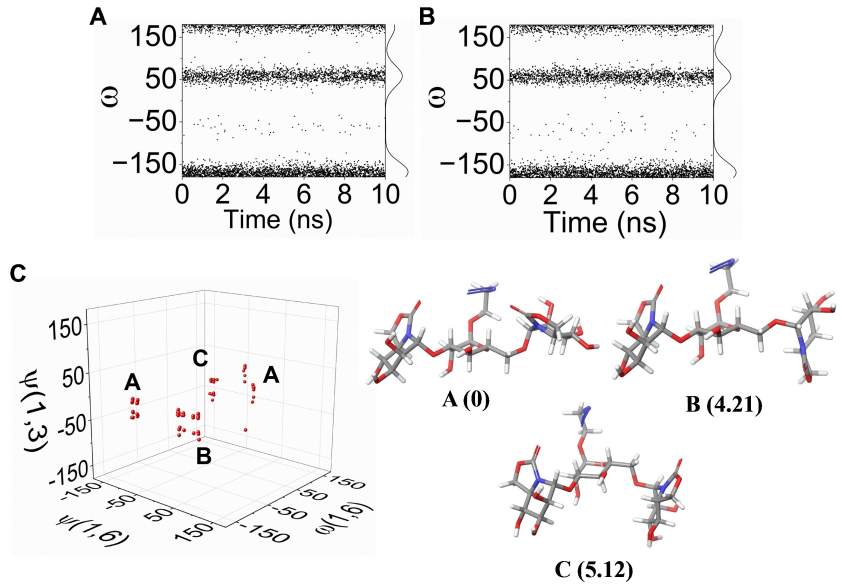

Figure 5. A and B) Evolution of the dihedral angle $\omega_{B,A}$ for the OMJ_2Man and Man_3 (pseudo)glycosides **9** and **8**, respectively, during the MC/SD simulation. C) ($\psi_{C,A}$,$\psi_{B,A}$,$\omega_{B,A}$) map obtained after MC/SD/MM for the OMJ_2Man pseudoglycoside **9** and representation of the minimum energy conformations for clusters A, B and C. Energy values relative to the absolute minimum are given in parenthesis.

180°) and *gauche-gauche* (*gg*; $\omega_{B,A} = 60°$). Based on the MC/SD data followed by multiple minimization (MC/SD/MM), a 3D ($\psi_{C,A}$,$\psi_{B,A}$,$\omega_{B,A}$) map was constructed (Figure 5C), revealing conformers that could be classified into three clusters (A–C). Clusters A and B mainly consisted of *gt* conformers, with cluster A being the most energetically favorable (0 kJ mol^{-1}) and cluster B slightly higher in energy (4.2 kJ mol^{-1}). Cluster C comprised *gg* conformers, which were energetically less favored (5.1 kJ mol^{-1}).

The experimental interproton distances H1^{C}/H3^{A} and H1^{B}/H6a^{A}, determined from NOESY experiments, exhibited good agreement with the calculated distances from either MC/SD or MS/SD/MM. However, a slight discrepancy was observed for the latter, which can be attributed to the high flexibility of the α(1,6) glycosidic linkage (Table 2 and Supporting Information, Figures S58–S61 and Table S3).

The conformational behavior of the Man_5 glycoside **10** can be rationalized as a combination of the previously discussed properties of the disaccharide derivative **1**-OMe concerning the two α(1,2)-linked terminal mannobiose moieties, and the Man_3 glycoside **8**, with respect to the internal α(1,3) and α(1,6) glycosidic linkages. The MCMM search revealed that the linear disaccharide segments can adopt both *S* and *E* conformations. In contrast, the branched portion displayed greater flexibility, with the ϕ angles oscillating around −50° and the ψ torsions exhibiting positive and negative values. The MC/SD results supported the presence of an equilibrium among these conformations (Supporting Information, Figure S62). The hemimimetic $(OMJMan)_2Man$ glycoside **11** exhibited a similar pattern, with slightly increased flexibility in the ϕ dihedral angles, resulting in a small yet significant population of non-exoanomeric conformations, as observed in the pseudotrisaccharide OMJ_2Man **9**. The MC/SD simulations further confirmed the presence of rapid conformational equilibria for the glycosidic linkages, specifically the ω torsion of the α(1,6) linkage shifting between the *gg* and *gt* orientations (Figure 6).

The quantitative analysis of interproton distances obtained from ROESY experiments corroborated the calculated distances and emphasized the similarity between the conformational properties of the Man_5 and $(OMJMan)_2Man$ moieties in glycosides **10** and **11**, respectively (Table 3 and Supporting Information, Figures S63, S64, S66 and S67). Upon MC/SD/MM minimization, the conformers of the Man_5 derivative **10** could be classified into five clusters (A–E; Figure 7A and Supporting Information, Figure S65), while $(OMJMan)_2Man$ derivative **11** conformers formed three clusters (A–C; Figure 7B and Supporting Information, Figure S68). Cluster A represented the global energy minimum for both compounds and exhibited very similar characteristics, with *gt* orientations around the α(1,6) ω torsion (Figure 6C and D). Conformers with *gg* orientations possessed significantly higher energies. All Man_5 (**10**) conformers adopted the *S* conformation at the mannobiose unit on the α(1,3)-linked arm, while the α(1,6)-linked arm displayed a mixture of *S* and *E* conformations. However, in the case of $(OMJMan)_2Man$ (**11**), the OMJMan residue on the α(1,3)-linked arm assumed the *S* conformation exclusively in the global minimum A.

Collectively, the computational and NMR data discussed above highlight that the substitution of peripheral α-D-mannopyranoside units with sp^2-iminosugar motifs in Man_2, Man_3, and Man_5 does not significantly alter their conformational properties. Although these hemimimetics exhibit slightly higher conformational flexibility, the relative distribution of conformers and their corresponding equilibria remain quite similar, establishing them as true conformational mimics.

Table 2. Theoretical (MC/SD and MC/SD/MM) and experimental (NOESY) diagnostic interproton distances (*d*) for the OMJ_2Man pseudoglycoside **9**.

Proton pair	$d_{MC/SD}$ [Å]	$d_{MC/SD/MM}$ [Å]	d_{Exp} [Å]
H-1^{C}/H-3^{A}	2.34	2.41	2.38
H-1^{B}/H-6a^{A}	2.54	2.40	2.91

Comparative evaluation of the ConA binding abilities of HMO hemimimetics by enzyme-linked lectin assay (ELLA)

The above commented studies have shown that all accessible conformations of the natural mannooligosaccharides Man_2, Man_3, and Man_5 are equally accessible for the synthesized OMJ-based analogues. Therefore, it is anticipated that the analogues can adopt the necessary conformation for binding to lectin receptors that recognize canonical HMO-related partners. The configurational pattern and the secondary hydroxyl group profile are identical. However, there are notable structural differences in the primary position region between Man and OMJ units, such as the anchor of the C5-C6 dihedral angle in the *gt* conformation due to the presence of a five-membered carbamate ring and the absence of the 6-OH, which is replaced by a carbonyl group. These modifications may modulate the interactions with amino acids at the primary and/or secondary carbohydrate binding sites in lectin partners.

Table 3. Theoretical (MC/SD) and experimental (ROESY) diagnostic interproton distances (*d*) for the Man_5 and $(OMJMan)_2Man$ derivatives **10** and **11**.

Proton pair	$d_{MC/SD}$ for 10 [Å]	d_{Exp} for 10 [Å]	$d_{MC/SD}$ for 11 [Å]	d_{Exp} for 11 [Å]
H-1D/H-2B	2.30	2.55	2.34	2.39
H-1E/H-2 C	2.30	2.67	2.34	2.46
H-1 C/H-3 A	2.31	2.07	2.30	2.13
H-1E/H-1 C	–	–	3.31	2.39
H-1B/H-6 A	2.93	3.03	2.45	2.20

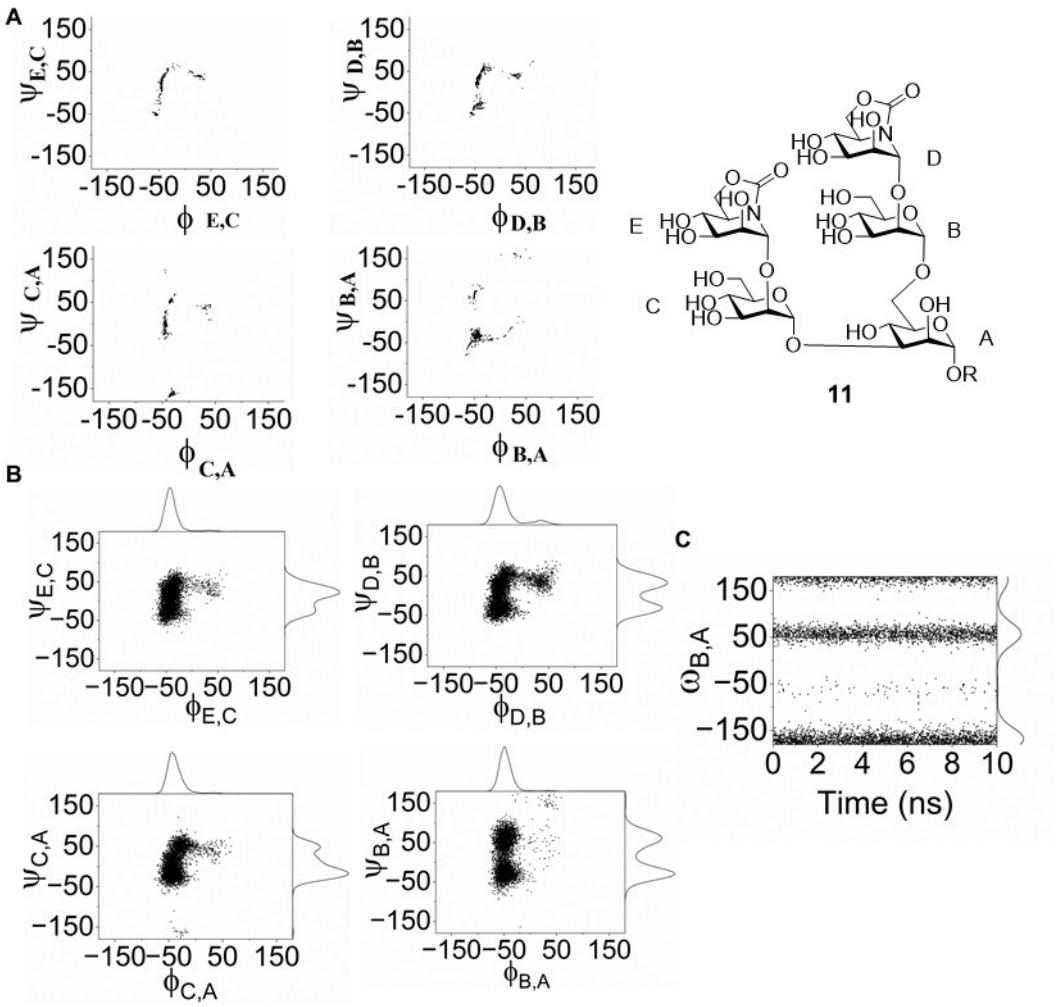

Figure 6. A) Structure of the $(OMJMan)_2Man$ derivative **11** with indication of the intermonosaccharide connectivity. (ϕ,ψ) maps obtained by the conformational search (MCMM/OPLS3e force field). B) (ϕ,ψ) map obtained by MC/SD simulation. C) Evolution of the dihedral angle $\omega_{B,A}$ during the MC/SD simulation.

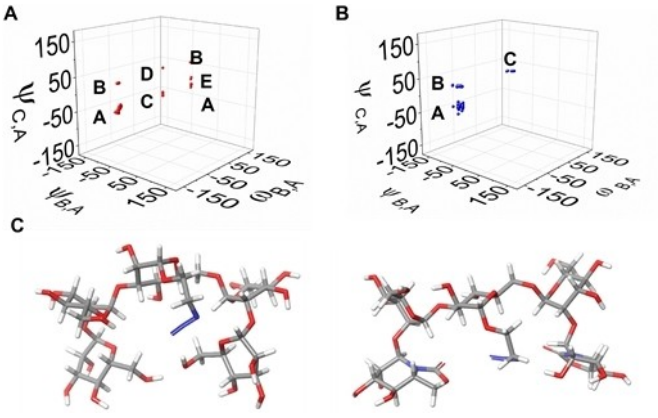

Figure 7. A and B) $(\psi_{C,A},\psi_{B,A},\omega_{B,A})$ maps obtained by MC/SD/MM calculations for the Man_5 and $(OMJMan)_2Man$ (pseudo)glycosides **10** and **11**, respectively. C and D) Representation of the absolute minimum energy conformations (clusters A) from the above $(\psi_{C,A},\psi_{B,A},\omega_{B,A})$ maps for **10** and **11**.

ConA, an extensively studied plant lectin, has played a significant role in advancing our understanding of multivalency. Many concepts derived from studies on multimannoside binding to ConA can be extrapolated to mannose-specific lectins in animals, despite their structural differences. This highlights the universal mechanisms underlying affinity enhancement through the multivalent effect. Notably, ConA, like DC-SIGN and langerin, can bind to Man_2 motifs in two distinct modes, positioning either the nonreducing or the reducing unit at the CRD. In this study, the enzyme-linked lectin assay (ELLA)[33] was employed to investigate the impact of replacing mannose units with OMJ motifs on complex formation with ConA. ELLA determines the ability of the tested glycoligand to compete with a reference ligand, which is immobilized on the microplate well (in this case, yeast mannan), for binding to the target lectin, which is labelled with an enzyme that catalyzes a reaction providing a suitable readout. In our case, we used horseradish peroxidase-labelled ConA (HRP-ConA). The use of horseradish peroxidase as a label mitigates crosslinking phenomena due to its large size. Therefore, ELLA is expected to provide information on the interaction with a single carbohydrate binding site in the lectin, eliminating potential aggregation effects.[34]

Figure 8 presents the ELLA plots and the corresponding IC_{50} values obtained for the series of (pseudo)di-, tri-, and pentasaccharides against HRP-ConA included in this work. It is evident that ConA does not recognize the pseudodisaccharide composed exclusively of the sp^2-iminosugar, namely OMJ_2. Indeed, a control experiment using the monosaccharide analog OMJ confirmed that this motif is not a ligand for ConA (data not shown). This finding aligns with the established understanding of the minimal structural requirements for ConA binding, which necessitate the presence of the diequatorial OH3/OH4 hydroxyls and the primary OH6 hydroxyl.[35] Surprisingly, the hemimimetic OMJMan demonstrated significantly enhanced ConA ligand efficacy compared to the monovalent reference, ManOMe, approaching the binding efficiency of Man_2. In other words, the nonreducing OMJ unit reinforces the recognition of the reducing Man unit. However, docking experiments did not reveal favorable secondary interactions between the sp^2-iminosugar and the neighboring amino acids within the carbohydrate recognition domain (CRD) (Supporting Information, Figure S82). One possible explanation is that once the Man moiety is situated at the CRD, rapid exchange with the OMJ unit at the protein surface becomes facilitated, even if the latter is a very poor ligand. This "reduction of dimensionality" mechanism has also been proposed to operate in heteromultivalent biological systems, leading to an increase in the half-life of the bound state.[18,36]

In ELLA conditions, the Man_3 glycoside **8**, for which ConA possesses an extended binding site,[37] exhibits 20-fold higher HRP-ConA binding affinity than ManOMe. However, binding is completely abolished for the hemimimetic OMJ_2Man glycoside derivative **9**, which lacks the primary hydroxyls. In sharp contrast, the Man_5 and $(OMJMan)_2Man$ glycosides **10** and **11** demonstrate similar behavior in ELLA, displaying approximately 100-fold higher potency than the Man_2 and OMJMan glycosides **1** and **3**, respectively. This consistency can be attributed to the divalent presentation of the (pseudo)mannobiose motif. In other words, both the α(1,3)- and α(1,6)-linked arms in Man_5 and $(OMJMan)_2Man$ maintain the (hetero)divalent "in line" ligand character. Molecular docking experiments conducted on the Man_5 glycoside **10**/ConA complex support the notion that a nonreducing Man unit is positioned at the CRD, preferably the one on the α(1,3)-linked arm. A similar situation is observed for the $(OMJMan)_2Man$ glycoside **11** (Supporting Information, Figure S83). These findings align with the crystal structure reported for the corresponding complex with the N-acetylglucosamine-terminated pentasaccharide β-GlcNAc-(1→2)-α-Man-(1→3)-[β-GlcNAc-(1→2)-α-Man-(1→6)]-Man ($GlcNAc_2Man_3$).[38]

Comparative evaluation of DC-SIGN and langerin binding to Man_3/OMJ_2Man and Man_5/$(OMJMan)_2Man$ (pseudo)oligosaccharides by NMR, molecular docking and surface plasmon resonance (SPR)

In the context of the interaction between the Man_2 or OMJMan glycosides **1** or **3** and DC-SIGN and langerin, previous studies utilizing NMR transfer techniques, including transferred-NOESY (tr-NOESY) and saturation-transfer difference (STD) NMR, and computational techniques have revealed that the CRD of these lectins can be occupied by either the nonreducing Man/OMJ unit or the reducing Man unit. Binding involves coordination to the Ca^{2+} cofactor through two adjacent hydroxyl groups in a trans diequatorial disposition and, unlike ConA, the presence of the primary OH6 hydroxyl is not essential for efficient binding. DC-SIGN exhibits a preference for the binding mode involving the reducing monosaccharide, while langerin favors the opposite pose.[14]

Analysis of the tr-NOESY spectra for Man_3 glycoside **8** in the presence of DC-SIGN and langerin revealed the characteristic sign change of cross-peaks, indicating the transient formation of the high molecular weight complex and therefore the interaction with the protein (Supporting Information, Figure S69A). This phenomenon was also observed for the OMJ_2Man glycoside **9**/DC-SIGN pair (Supporting Information, Figure S69B). However, in the case of **9** in the presence of langerin, only a subset of cross-peaks exhibited sign changes. This suggests a weaker interaction that involves a smaller area of the pseudotrisaccharide molecule accompanied by a variation on local flexibility (Supporting Information, Figure S69B). Binding of both **8** and **9** to DC-SIGN was confirmed by STD experiments (Figure 9A and C and Supporting Information, Figures S71 and S72). Due to extensive signal overlapping, it

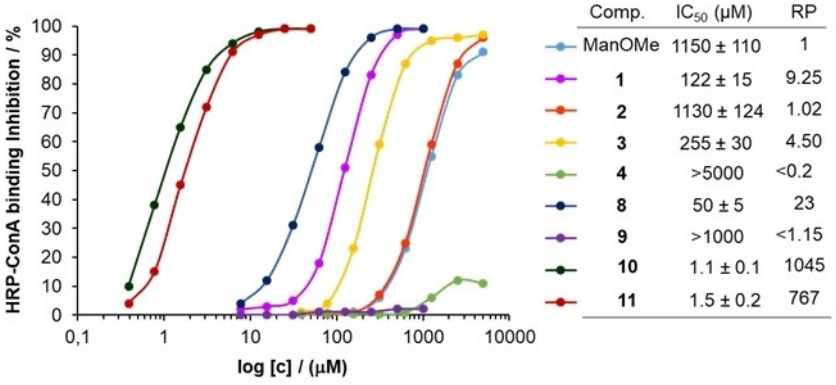

Figure 8. ELLA plots for the inhibition of HRP-ConA to yeast mannan by compounds **1**–**4** and **8**–**11**, with indication of the corresponding IC_{50} values and relative potencies (RP; referred to ManOMe). Data for methyl α-D-mannopyranoside (ManOMe) are included as a monovalent Man reference.

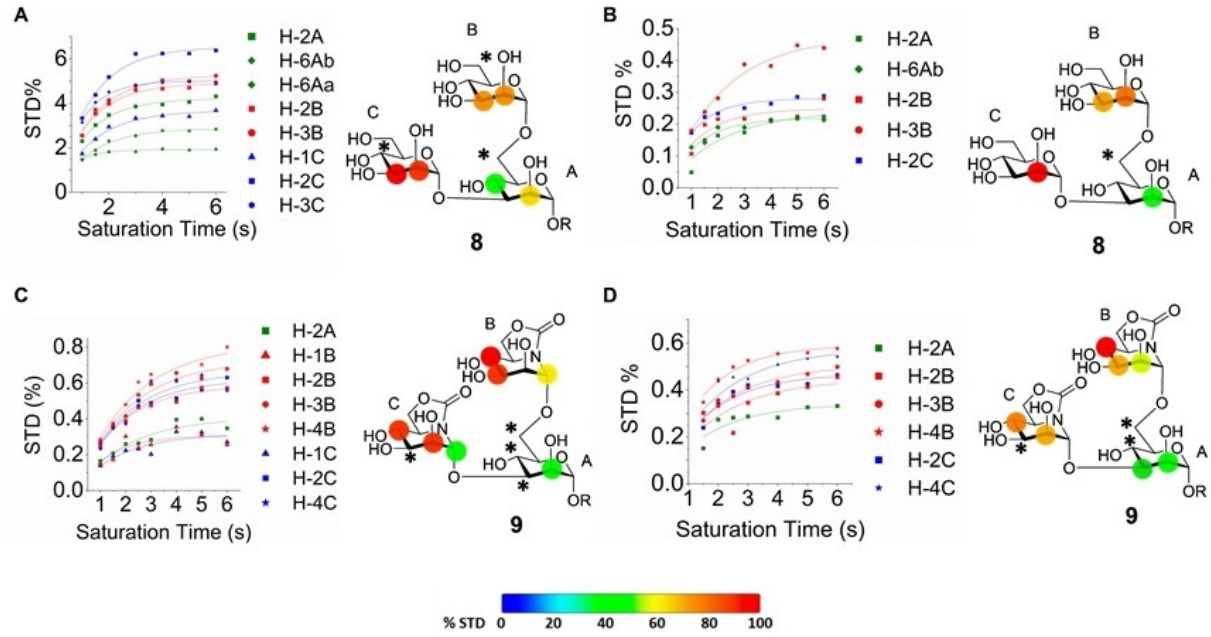

Figure 9. A and B) STD plots for the Man_3 glycoside **8** faced to DC-SIGN and langerin, respectively. C and D) STD plots for the OMJ_2Man pseudoglycoside **9** faced to DC-SIGN and langerin, respectively. The structures of the ligands, with indication of the normalized STD (%; color scale) derived from the initial slopes, are shown. Protons that are observed in the STD spectra but cannot be integrated due to overlapping are labelled with an asterisk.

was challenging to map the complete epitopes; however, the data indicate that the nonreducing residues are primarily involved in the recognition process. Transfer of saturation was found to be larger for the α(1,3)-linked residue in both cases, suggesting that this unit interacts more favorably with the lectin. Nevertheless, the existence of a dynamic equilibrium between two alternative binding modes, with the α(1,3)- or α(1,6)-linked Man or OMJ moiety coordinating the Ca^{2+} cation through OH3 and OH4, cannot be ruled out. In the case of STD experiments with langerin, saturation values of the ligand protons were significantly lower compared to the analogous experiments with DC-SIGN (Figure 9B and D). Nonetheless, the data are consistent with the existence of a similar equilibrium between the two binding modes.

The examination of supramolecular complex structures obtained through molecular docking, which are consistent with experimental NOE contacts in the bound state, provides insights to rationalize the observations. In the most favorable binding pose, Man_3 glycoside **8** binds to DC-SIGN in a pincer-like fashion, where both nonreducing residues interact simultaneously with the protein, while the branched reducing residue does not significantly participate in binding. The α(1,3)-linked residue occupies the metal coordination site, whereas the α(1,6)-linked residue establishes hydrogen bonds and van der Waals interactions with neighboring amino acids, such as Asn344, Arg345, and Asn362 (Figure 10A). This binding mode lines up with previous reports on Man_3/DC-SIGN interactions[39] and is supported by crystal structures of the $GlcNAc_2Man_3$/DC-SIGN[40] and Man_4/DC-SIGN complexes.[41] A similar binding mode is observed for the trisaccharide mimetic OMJ_2Man glycoside **9**, although the interactions of the α(1,6)-linked residue with Arg345, which involve the primary hydroxyl in Man_3, are not observed (Figure 10B). In contrast, when considering langerin, the docking results suggest binding modes for **8** and **9** that resemble those reported for Man_2,[42] with only one of the nonreducing residues occupying the CRD. Additional interactions at secondary sites do not contribute to binding in either case (Figure 10C and D).

tr-NOESY spectra for the free Man_5 and $(OMJMan)_2Man$ glycosides **10** and **11** exhibited cross-peaks with the same sign as those in the diagonal, which is compatible with large molecules. In addition, the NOESY peaks in presence of lectin remained unchanged compared with the free ligands, consequently we were unable to provide qualitative information on the formation of lectin complexes (see the Supporting Information for a detailed description of the NOESY NMR experiments). In the case of the **10**/DC-SIGN pair, STD results demonstrated significant saturation of all protons in the two mannobiose antennae, supporting complex formation (Figure 11A). Although some signals experienced overlapping, it was evident that the intensity of the STD signals from the internal Man residues, particularly the α(1,3)-linked residue, was higher. The best binding pose obtained through molecular docking closely resembled that reported for the $GlcNAc_2Man_3$/DC-SIGN complex,[40] with the α(1,3)-linked Man coordinated to the metal center through OH3 and OH4. The external Man unit in this branch was accommodated on Val351, similar to the binding observed for Man_2,[42] while the α(1,6)-linked mannobiose segment oriented towards Phe313 and Ser360, establishing several van der Waals and hydrogen bond contacts (Figure 11B and Supporting Information, Figure S73). The corresponding STD and molecular docking experiments for the

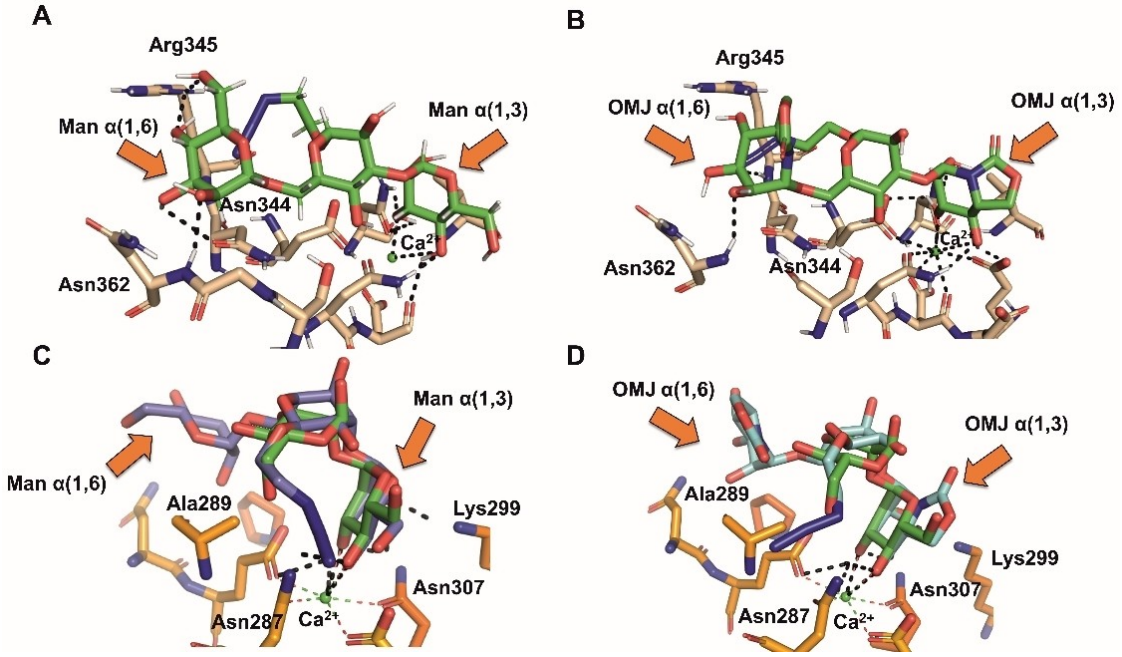

Figure 10. Predicted binding mode for ligands A) **8** and B) **9** to DC-SIGN (coordinates from PDB 1 K9I) obtained by docking. Predicted binding mode for ligands C) **8** and D) **9** to langerin (coordinates from PDB 3P5F) obtained by docking, superimposed with the crystal structure of the Man_2/langerin complex[42] (carbons are represented in green for Man_2 and in lilac or light blue for **9**).

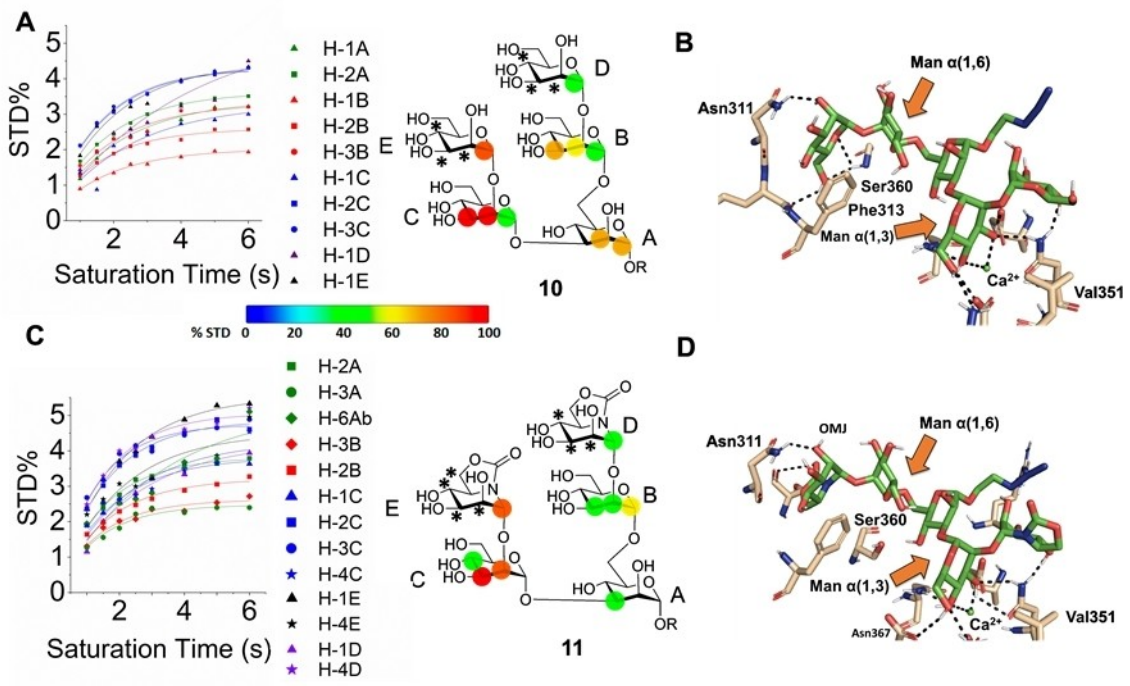

Figure 11. A) STD growth plots for the Man_5 glycoside **10** faced to DC-SIGN and epitope map. B) Predicted binding mode for ligand **10** to DC-SIGN (coordinates from PDB 2IT5) obtained by docking. C) STD growth plots for the $(OMJMan)_2Man$ pseudopentasaccharide **11** faced to DC-SIGN and epitope map. D) Predicted binding mode for ligand **11** to DC-SIGN (coordinates from PDB 2IT5) obtained by docking. The structures of the ligands, with indication of the normalized STD (%, color scale) derived from the initial slopes, are shown. Protons that are observed in the STD spectra but cannot be integrated due to overlapping are labelled with an asterisk.

$(OMJMan)_2Man$ pseudopentasaccharide **11** revealed a nearly identical binding mode to DC-SIGN, indicating that the sp^2-iminosugar hemimimetic mirrors the natural HMO **10** (Figure 11C and D and Supporting Information, Figure S74).

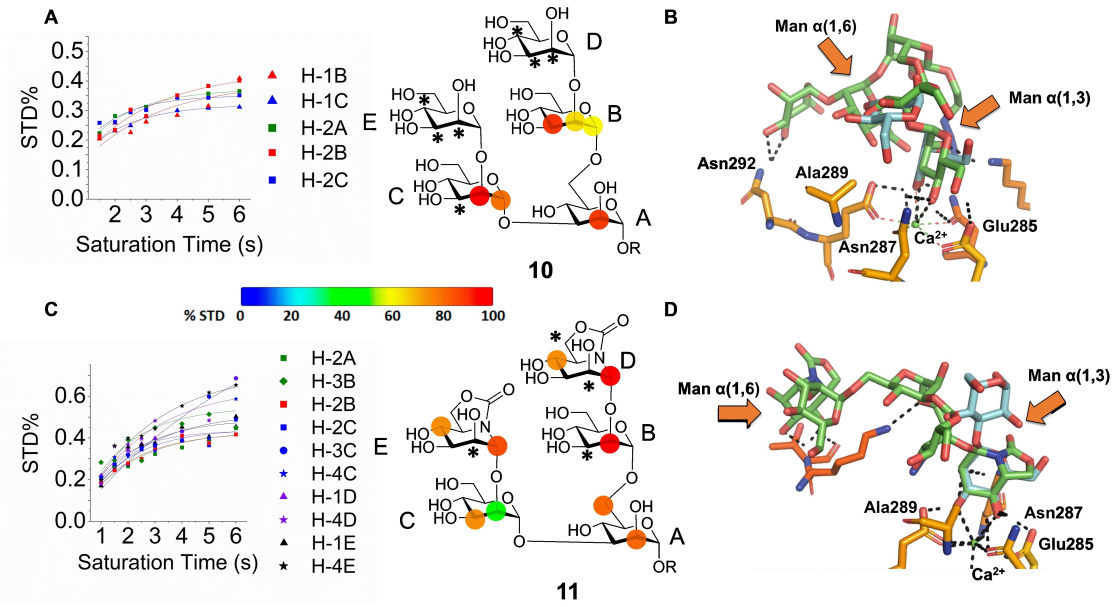

Figure 12. A) STD growth plots for the Man_5 glycoside **10** faced to langerin and epitope map. B) Predicted binding mode for ligand **10** to langerin (coordinates from PDB 3P5D) obtained by docking, superimposed with X-RAY Man_2/langerin. C) STD growth plots for the $(OMJMan)_2Man$ pseudopentasaccharide **11** faced to langerin and epitope map. D) Predicted binding mode for ligand **11** to langerin (coordinates from PDB 3P5D) obtained by docking, superimposed with X-RAY Man_2/langerin. The structures of the ligands, with indication of the normalized STD (%) derived from the initial slopes, are shown. Protons that are observed in the STD spectra but cannot be integrated due to overlapping are labelled with an asterisk.

STD experiments likewise were consistent with Man_5 and $(OMJMan)_2Man$ glycosides **10** and **11** binding to langerin. Unfortunately, only partial binding epitope maps could be drawn, due to substantial signal overlap (Figure 12A and C and Supporting Information, Figure S77 and S78). Since the integrable signals differ for **10** and **11**, a direct comparison can be misleading. Indeed, the ^{1}H-STD NMR spectra (Supporting Information, Figure S77 and S78) showed that the α(1,2)-linked Man or OMJ units were the ones primarily involved in complex formation in both cases. This is consistent with docking calculations (Figure 12B and D). Nevertheless, participation of the internal Man units cannot be discarded. The ligands were found to exhibit less contacts with langerin as compared with DC-SIGN, which is in accord with the greater challenges faced by langerin in accommodating larger ligands.

The biomimetic properties of the hemimimetic compounds **9** and **11** were further validated through surface plasmon resonance (SPR) studies, (see the Supporting Information for the corresponding sensorgrams) which aimed to assess their competitive inhibition of DC-SIGN and langerin binding to mannosylated bovine serum albumin (Man-BSA). The reference mannooligosaccharide derivatives **8** and **10** were employed as controls in the experiments. Table 4 displays the corresponding IC_{50} values for the inhibitory activity of the compounds. In order to facilitate comparison, IC_{50} values for Man_2 and OMJMan glycosides **1** and **3** are also provided in the table.

In terms of DC-SIGN binding, the pseudotrisaccharide OMJ_2Man glycoside **9** (IC_{50} = 593 μM) exhibited higher affinity towards this lectin compared to the mannotrisaccharide derivative **8** (IC_{50} = 700 μM). This enhanced binding can be attributed to the increased conformational flexibility of the former, which enables a better adaptation to the pincer-like binding mode mentioned earlier. Additionally, the dynamic interconversion between the α(1,3)-linked and α(1,6)-linked OMJ residues coordinating the Ca^{2+} cation may occur more readily in OMJ_2Man. Concerning Man_5 and $(OMJMan)_2Man$ glycosides **10** and **11**, their affinity trend and IC_{50} values (209 and 265 μM, respectively) can be interpreted in terms of their divalent nature compared to Man_2 and OMJMan glycosides **1** and **3** (IC_{50} values 590 and 1060 μM, respectively). The overall conclusion is that substituting the nonreducing Man residue with OMJ in the oligosaccharides does not significantly impact the binding properties to DC-SIGN, which aligns with the NMR and computational data.

The inhibitory potencies of the (pseudo)glycoligands **1**, **3**, **8**–**11** towards langerin, as assessed by SPR, were lower

Table 4. SPR-derived IC_{50} values for the inhibition of DC-SIGN and langerin binding to surface-immobilized BSA-Man by compounds **8**–**11**. Data for compounds **1** and **3**, obtained in a previous study,[14] are included for comparison. DC-SIGN vs langerin selectivity values, obtained from the corresponding IC_{50} (langerin)/IC_{50} (DC-SIGN) quotients, are also shown.

Compound	IC_{50} (DC-SIGN; μM)	IC_{50} (langerin; μM)	DC-SIGN vs langerin selectivity
1	590 ± 20[a]	6990 ± 200[a]	11.7
3	1060 ± 100[a]	12900 ± 200[a]	12.2
8	700 ± 1	1838 ± 19	2.6
9	593 ± 3	3153 ± 26	5.3
10	209 ± 1	600 ± 3	2.9
11	265 ± 1	678 ± 3	2.6

[a]Data from ref. [14].

compared to DC-SIGN for all ligands tested. Notably, substituting Man with OMJ at the nonreducing ends of the ligands consistently resulted in impaired langerin binding. However, despite this detrimental effect, the observed IC_{50} trend for the hemimimetic ligands **3**, **9** and **11** closely mirrored that of the parent mannooligosaccharides **1**, **8** and **10**, indicating that (hetero)multivalent effects operate similarly in both ligand series.

The ratio between the IC_{50} values obtained for langerin and DC-SIGN provides valuable insights into the selectivity of each ligand towards these receptors. Our data suggests that as the size of the HMO-related pseudooligosaccharides increases, the selectivity of DC-SIGN over langerin decreases. Specifically, when considering the (pseudo)di- (**1** and **3**) and (pseudo)penta-saccharides (**9** and **10**), which can be regarded as mono- and divalent species of Man_2 (or OMJMan), an enhancement in binding efficiency is accompanied by a reduction in selectivity. No significant impact of replacing the peripheral Man units into OMJ motifs is seen.

Synthesis of multivalent OMJMan conjugates with varied architectures and comparative evaluation of their ConA binding abilities by ELLA

In our previous communication,[14] we used a βCD scaffold to access the (pseudo)disaccharide multiconjugates OMJMan-βCD (**20** and **22**) and Man_2-βCD (**19** and **21**) (Figure 13). In that case, the presence of OMJ instead of Man at the periphery of the heptavalent tetradecavalent glycocluster resulted in total DC-SIGN over langerin selectivity. This is sharply different to the results above discussed for the (pseudo)penta-saccharides **9** and **10**. The discrepancy can be attributed to the fact that the influence of valency and architectural features on (hetero)multivalent effects is substantial. In order to gain a more comprehensive understanding of how these parameters differentially affect Man_2 and OMJMan displays binding to the lectins, we next undertook the synthesis and evaluation of an expanded library of OMJMan multivalent derivatives on platforms with varying topologies.

The new (pseudo)glycoclusters prepared in this work are depicted in Figure 14 (first generation) and Figure 15 (second generation derivatives). First generation compounds **23**–**28** were synthesized using copper(I)-catalyzed azide-alkyne coupling (CuAAC) reactions employing three different poly(alkyne)-equipped scaffolds: (a) the cyclodecapeptide scaffold **37**,[43] (b) the polylysine dendron **38**[43] and (c) the planar cyclophosphazene **39**.[44] The multiconjugation reactions of **37**–**39** with Man_2 or OMJMan α-azidoethyl glycosides (**1** or **3**) were performed in dimethylformamide (DMF)-phosphate buffered saline (PBS; pH 7.4) in the presence of tris(3-hydroxypropyl-triazolylmethyl)amine (THPTA). A combination of cupric sulfate and ascorbic acid was used to generate the Cu(I) catalyst, resulting in the formation of tetravalent (**23**–**26**) and hexavalent (**27** and **28**) displays (Scheme 3).

Next, second-generation conjugates **29** and **30** were obtained by incorporating an N′-pentynoyl appendage on the unsubstituted lysine residue in (pseudo)glycocyclodecapeptides **23** and **24** (see Supporting Information, p. S15). The resulting alkyne-functionalized derivatives **40** and **41** were subjected to CuAAC with the structurally related tetrazide **42**[45] to yield the desired hexadecavalent compounds (Scheme 4). Similar transformations were carried out with the alkyne-functionalized polylysine (pseudo)glycodendrons **43** and **44**, obtained by N-pentynoylation of **25** and **26** (Supporting Information, p. S17), and tetrazides **42** and **45**,[46] resulting in the corresponding homologous hexadecavalent derivatives **31**, **32** and **33**, **34**, respectively (Scheme 4). Finally, N′-azidoacetylation of **25** and **26** with azidoacetic acid N-hydroxysuccinimide (NHS) ester (Supporting Information, p. S22) and CuAAC of the resulting

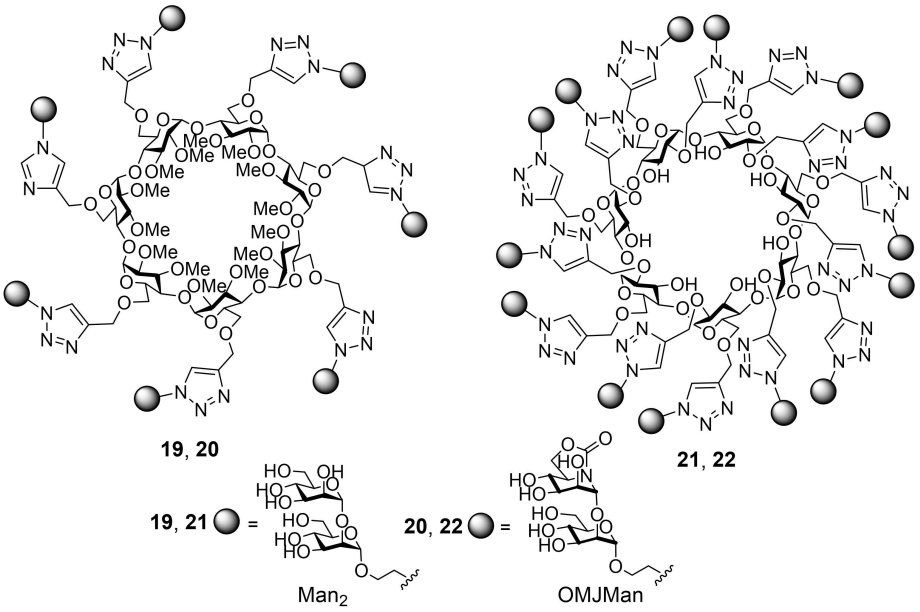

Figure 13. Structures of the βCD-scafolded (pseudo)glycoclusters previously synthesized **19**, **20** (heptavalent) and **20**, **21** (tetradecavalent).

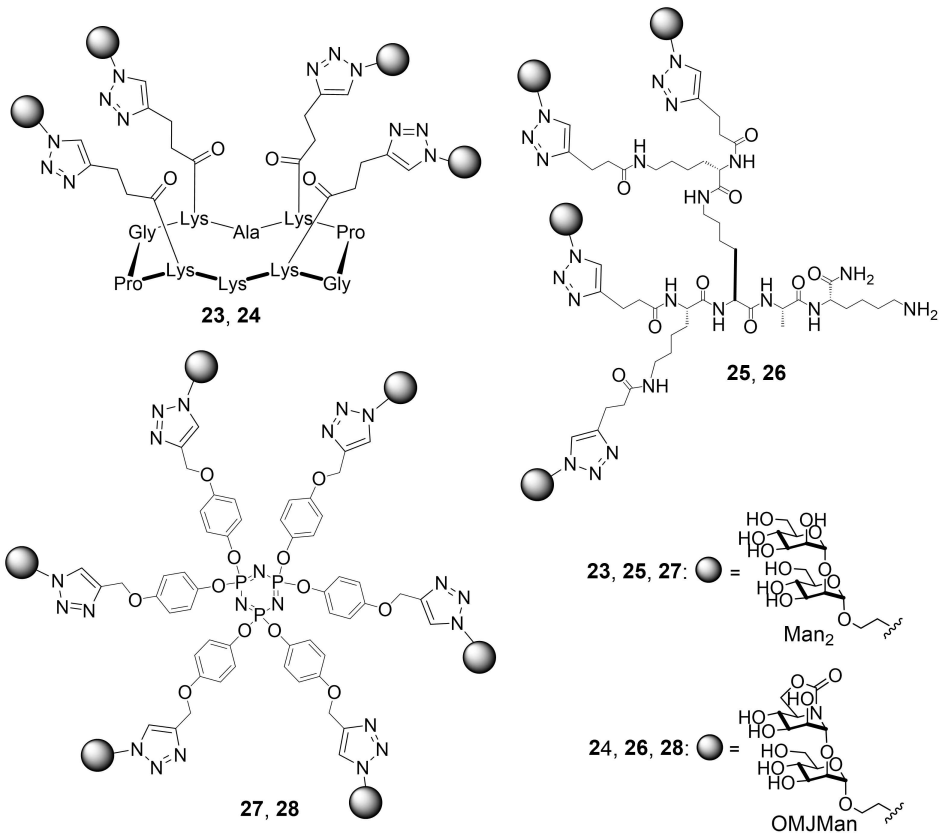

Figure 14. Structures of the first generation (pseudo)glycoclusters built on cyclodecapeptide (**23** and **24**; tetravalent), polylysine dendron (**24** and **26**; tetravalent) and cyclophosphazene (**27** and **28**; hexavalent) scaffolds.

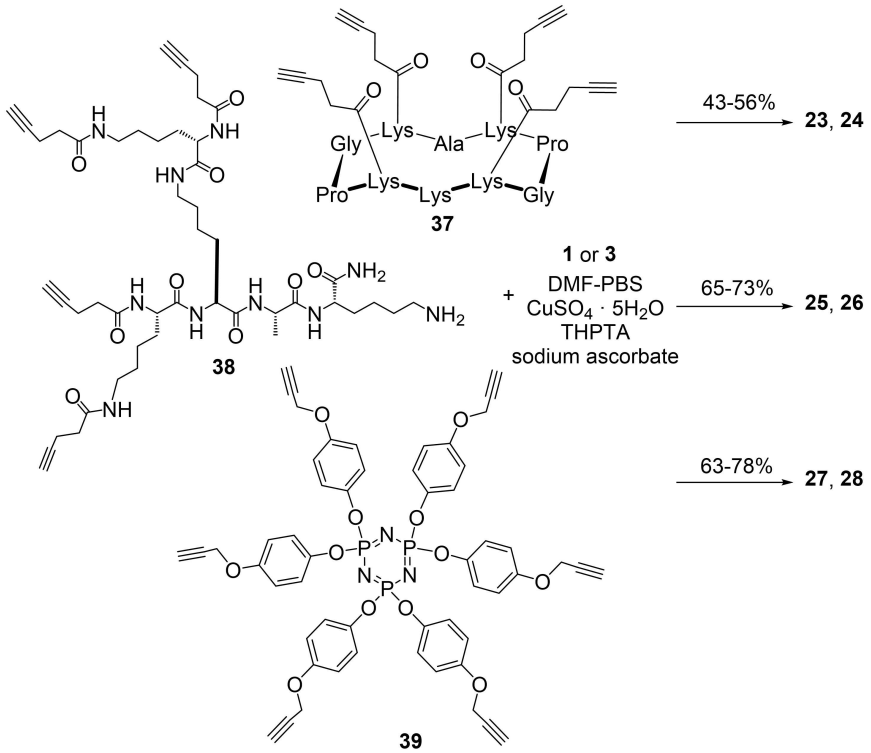

Scheme 3. Synthesis of the first generation (pseudo)glycoclusters **23**–**28**.

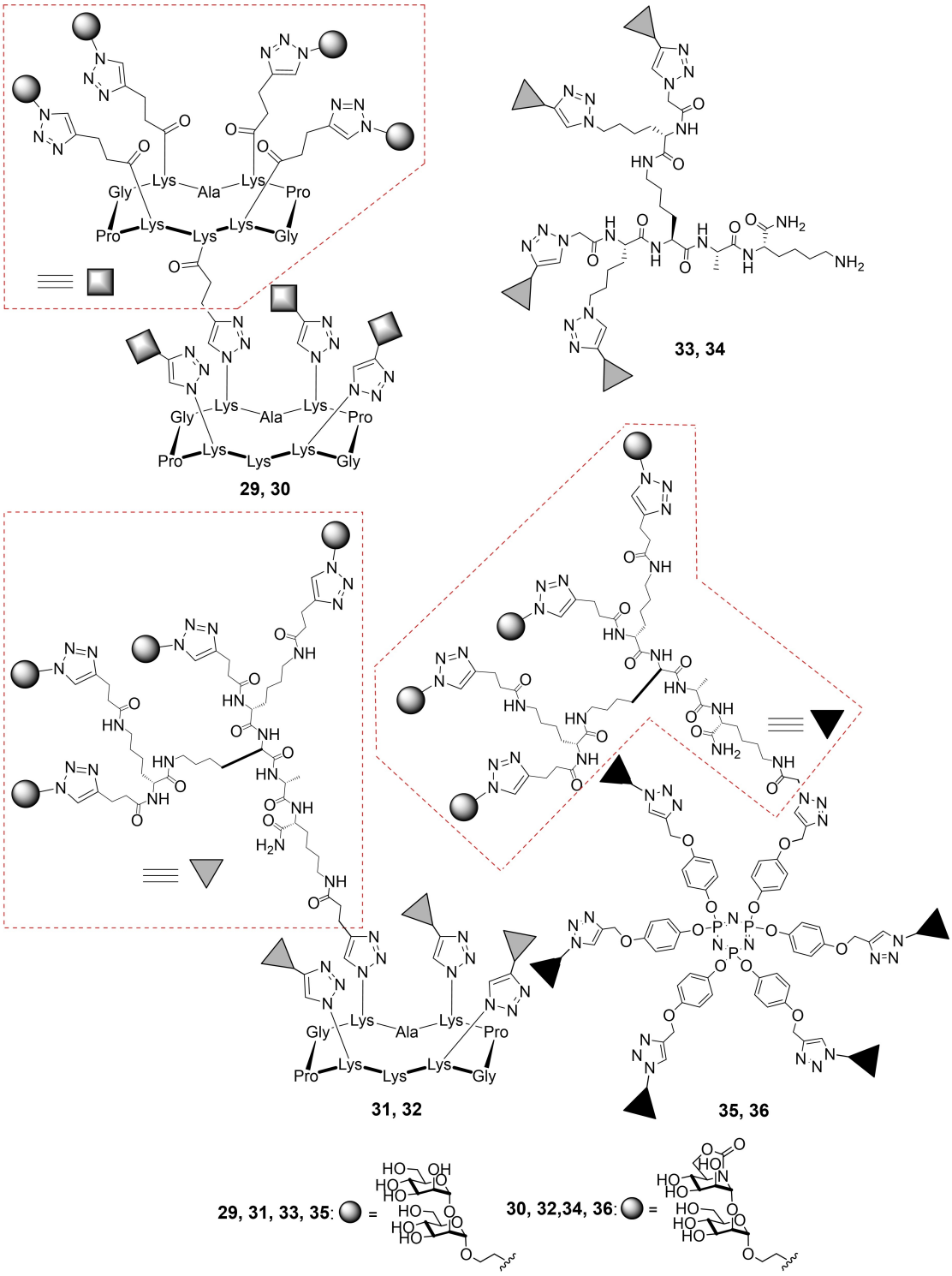

Figure 15. Structures of the second generation (pseudo)glycoclusters combining cyclodecapeptide/cyclodecapeptide (**29** and **30**; hexadecavalent), cyclodecapeptide/polylysine dendron (**31** and **32**; hexadecavalent), polylysine dendron/polylysine dendron (**33** and **34** (hexadecavalent) and polylysine dendron/cyclophosphazene (**35** and **36**; tetraeicosavalent) scaffolds.

(pseudo)glycodendritic azides **46** and **47** with the hexaalkynyl-phosphazene platform **39** provided the tetraeicosa Man_2 and OMJMan conjugates **35** and **36** (Scheme 4) The structure, homogeneity, and purity of all new compounds were confirmed by mass spectrometry (MS), reversed-phase (RP)-HPLC, ^{1}H, ^{13}C, and, when applicable, ^{31}P NMR (Supporting Information, Figures S1–S48).

The IC_{50} values obtained by ELLA for the inhibition of yeast mannan/HRP-ConA binding by the whole series of Man_2 and OMJMan multiconjugates **19**–**36** are summarized in Table 5 (see

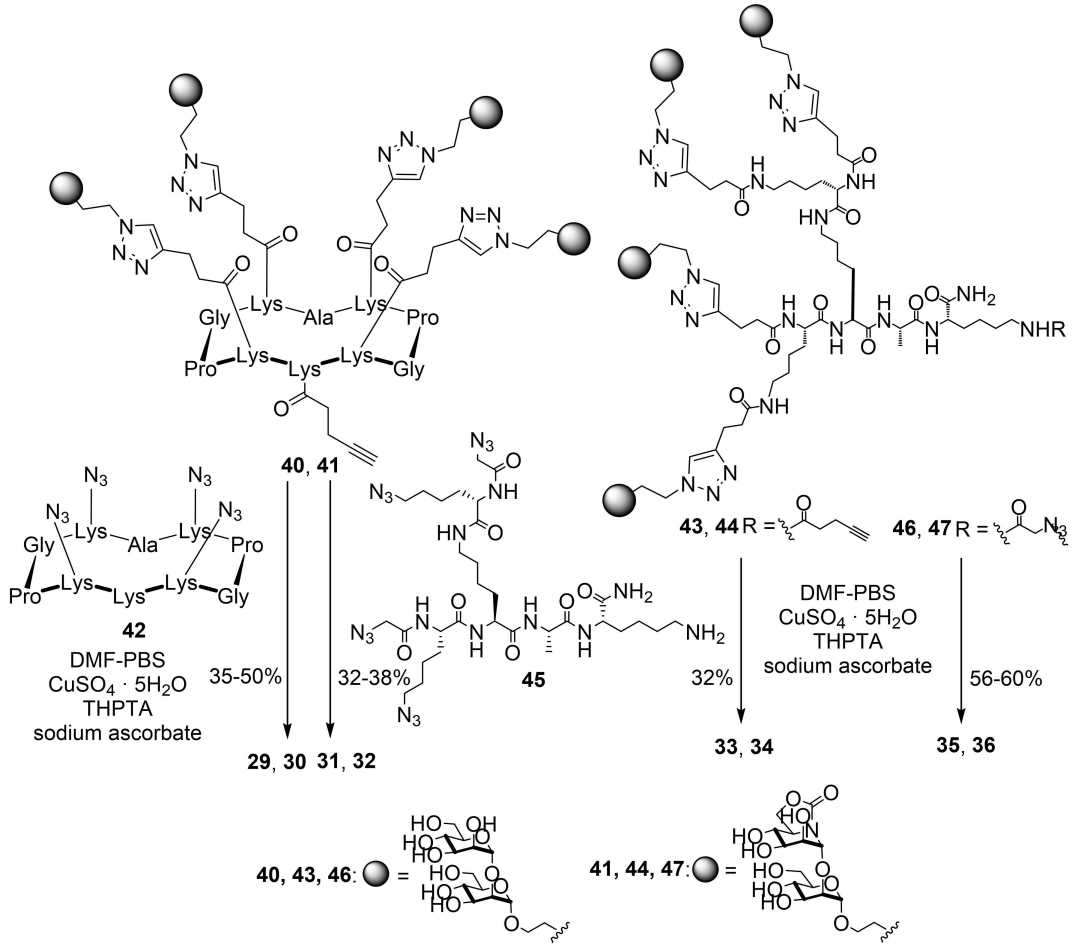

Scheme 4. Synthesis of the second generation (pseudo)glycoclusters **29**–**36**.

the Supporting Information, Figure S79–S81, for the corresponding inhibition plots). It should be noted that ELLA data tends to reach a plateau for strong lectin binders, primarily due to the inherent limitations of the technique in accounting for crosslinking and chelate contributions to the multivalent effect. Nevertheless, the overall results indicate that OMJMan benefits from multivalency similarly to Man_2. The extend of the inhibitory activity enhancement (relative potency, RP), normalized to that of the monovalent pseudodisaccharide (RP/n), depends on the valency and on the platform used. The hexadecavalent cyclodecapeptide-based OMJMan cluster **30** stood out among the second generation derivatives (RP/n = 10.6), whereas the hexavalent cyclophophazene conjugate **28** showed the highest RP/n value (6.64) among the first generation derivatives. By comparison, the increase in affinity with the number of epitopes is somewhat less pronounced for βCD conjugates (RP/n = 1.44 and 3.31, for the hepta and tetradecavalent OMJManclusters **20** and **22**, respectively; even much lower, 0.48 and 0.38, for the Man_2 conjugates **19** and **21**). This can be attributed to the higher degree of compaction of the substituents on the βCD rims, which may hinder the approachability of HRP-ConA and limit accessibility of the internal (nonreducing) Man unit to the CRD.[47]

Comparative evaluation of DC-SIGN and langerin binding to OMJMan pseudoglycoclusters by surface plasmon resonance (SPR)

Subsequently, we investigated the binding abilities of OMJMan pseudoglycoclusters towards DC-SIGN and langerin using SPR analysis. The obtained apparent dissociation constant (App K_D) values from the SPR sensorgrams are presented in Table 6. For the cyclodecapeptide-scaffolded tetravalent compound **24**, satisfactory curve fittings could not be achieved. Instead, we determined the IC_{50} values for the inhibition of the corresponding lectin binding to Man-BSA. It should be emphasized that in this case the binding of the ligand to the lectin occurs in the solution phase, whereas for K_D determinations it takes place on the surface. Therefore, any direct comparison between these two sets of data should be approached with caution.

The SPR data obtained for the first-generation clusters revealed App K_D (or IC_{50}) values in the micromolar range, whereas the second generation exhibited K_D values in the nanomolar range. Notably, considering that the valency is fourfold higher in the second generation series, the significant enhancement in binding affinity is consistent with the ability of the mannobioside mimetic OMJMan to leverage the multivalent

Table 5. IC_{50} values, relative potencies and normalized relative potencies for the inhibition of HRP-ConA to yeast mannan by compounds **19–36** determined by ELLA. Data for the monovalent Man_2 and OMJMan derivatives **1** and **3** are included for comparison.

Compound	Valency	IC_{50} [μM]	RP[a]	RP/n
1	1	122 ± 15	1	1
3	1	255 ± 30	1	1
19	7	36.1 ± 4.3	3.39	0.48
20	7	25.2 ± 3.0	10.2	1.44
21	14	23.7 ± 2.3	5.27	0.38
22	14	5.5 ± 1.5	46.36	3.31
23	4	20.5 ± 2.5	6.09	1.52
24	4	25.7 ± 8.3	9.92	2.48
25	4	23.4 ± 2.8	5.34	1.33
26	4	21.3 ± 2.5	11.97	2.99
27	6	3.9 ± 0.5	32.05	5.34
28	6	6.4 ± 0.7	39.84	6.64
29	16	0.31 ± 0.04	403	25.2
30	16	1.5 ± 0.2	170	10.6
31	16	5.4 ± 0.7	23.1	1.44
32	16	3.8 ± 0.5	34.1	4.19
33	16	1.2 ± 0.2	67.1	6.51
34	16	14.9 ± 0.9	104.2	1.07
35	24	1.2 ± 0.2	28.8	4.34
36	24	2.1 ± 0.3	121.4	5.06

[a] Folds of increase relative to the corresponding IC_{50} value for the monovalent Man_2 or OMJMan glycoside (**1** or **3**, respectively).

Table 6. SPR-derived apparent dissociation constant (App K_D) values for the OMJMan pseudoglycoclusters **26**, **28**, **30**, **32**, and **36** binding to DC-SIGN and langerin, and IC_{50} values for the inhibition of DC-SIGN and langerin binding to surface-immobilized BSA-Man by compound **24**. DC-SIGN vs langerin selectivity values are also shown. Data for the OMJMan/βCD conjugates **20** and **22** are included for comparative purposes.[14]

Compound	Valency	App K_D (DC-SIGN)	App K_D (langerin)	DC-SIGN vs langerin selectivity[a]
20	7	7.1 ± 0.6 μM	> 500 μM[b]	> 70.4
22	14	5.5 ± 1 μM	> 500 μM[b]	> 90.0
24	4	14.55 ± 0.05 μM[c]	7.68 ± 0.01 μM[c]	1.45
26	4	13.6 ± 1.6 μM	19.2 ± 1.7 μM	1.41
28	6	13.4 ± 0.2 μM	19.0 ± 1.9 μM	1.42
30	16	118 ± 28 nM	66 ± 13 nM	0.56
32	16	0.6 ± 0.1 nM	20 ± 3 nM	33.3
34	16	0.6 ± 0.1 nM	26 ± 4 nM	43.3
36	24	1.3 ± 0.2 nM	35 ± 3 nM	26.9

[a] Defined as App K_D (langerin)/App K_D (DC-SIGN) or IC_{50} (langerin)/ IC_{50} (DC-SIGN). [b] No binding detected at 500 μM. [c] IC_{50} value for the inhibition of the lectin binding to mannosylated bovine serum albumin (Man-BSA).

effect, as previously observed for ConA binding. Furthermore, the increase in valency had a remarkable impact on the selectivity between DC-SIGN and langerin. While the binding affinity for DC-SIGN was only slightly more favorable than for langerin for the smaller pseudoglycoclusters **24**, **26** and **28** (1.41 to 1.45-fold), the App K_D (langerin)/App K_D(DC-SIGN) ratio increased to 33.3, 43.3, and 26.9 for compounds **32**, **34**, and **36**, respectively. Interestingly, compound **30** exhibited reversed selectivity, demonstrating it to be an almost two-fold better ligand for langerin compared to DC-SIGN. This unexpected result could be attributed to non-specific interactions between the scaffold itself and the langerin-functionalized surface. Previous studies have shown that the contribution of the naked double cyclopeptide-based scaffold, without any glycoligand, accounts for up to one-third of the binding observed for a tetradecavalent mannobioside mimetic constructed on the same system. In contrast, this platform is only minimally recognized by DC-SIGN.[48]

It is also interesting to compare the findings presented in this study with previous data obtained for the hepta- and tetradeca-valent OMJMan/βCD conjugates **20** and **22**. In the latter case, the increase in valency did not lead to a strengthened multivalent effect against DC-SIGN. This result aligns with the observations made for ConA, reinforcing the idea that the access of the glycomimetic motif to the lectin CRD is significantly hindered when presented on the more compact βCD platform compared to other scaffolds. The less accessible CRD of langerin renders this lectin more susceptible to steric hindrance, resulting in a complete lack of binding.

Given the good performance of the Force Fields at reproducing the conformational properties of the HMO-related compounds **8**–**11**, we decided to apply a similar approach to model the more complex multivalent derivatives. Experimental details are given in the supplementary information. Figure 16 depicts representative structures for the heptavalent and tetradecavalent OMJMan-βCD (**20** and **22**) and Man_2-βCD (**19** and **21**) glycoclusters. Based on crystallographic structures we construct two models for the extracellular domains of DC-SIGN and langerin, with the CRD and the first module of the extracellular alpha helix connecting it with the membrane, E and F, respectively. The increase of the App K_D value on going from the heptavalent to the tetradecavalent derivatives can be ascribed to a classical multivalent effect: several situations in fast interconversion can display almost similar interactions (fast up-down rotation). Interestingly, close examination of the molecular models reveals that the rigid βCD platform hinders the access of the internal ("reducing") Man residue to the protein CRD (Figure 16). This provides a rational for the observed differences in the behaviour of the ligands relative to the two lectins: while the more open tetrameric arrangement of DC-SIGN enables the interaction with the external Man or OMJ residue as well as with the internal Man unit, trimeric langerin can only accommodate external Man residues. Consequently, langerin binding is banned for the OMJMan conjugates **20** and **22**.

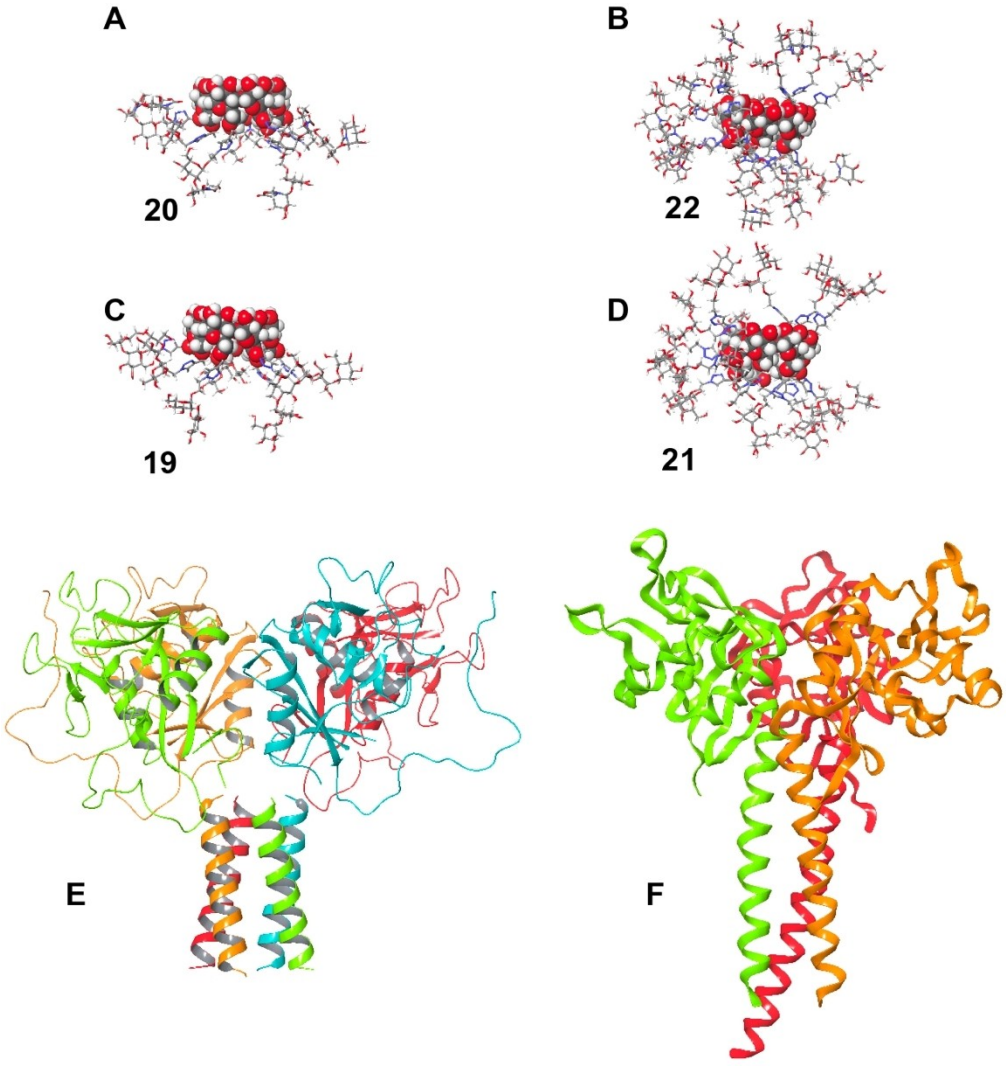

Figure 16. A–D) Representative molecular models of compounds **19**–**22**. E) Structure of DC-SIGN. F) Structure of langerin. Protein structures are taken from the PDB entries 1k9i and 3PQG with minor automatic modifications, while in the ligands the βCD ring is represented as CPK and the substituents as sticks.

The lack of selectivity in the case of multivalent OMJMan glycoclusters built on RAFT cyclodecapeptide, lysine-based dendrimer or cyclophosphazene platforms probably implies the participation of the internal Man residue on langerin binding. Inspection of the molecular models for the first-generation compounds **24**, **26** and **28** as well as for the second generation conjugates **32**, **34** and **36** indicates a much less compact architecture as compared with the βCD derivatives, supporting this hypothesis (Figure 17).

Conclusions

The results discussed in this manuscript provide a practical approach for the synthesis of HMO hemimimetics that faithfully replicate the substitution and configuration pattern of their natural counterparts. This general strategy is based on the concept of chemical mimicry, leveraging the unique stereoelectronic properties of sp^2-iminosugars. Specifically, the cyclic acylimine functionality exhibits glycosylation-like reactivity, controlled by the anomeric effect, enabling the implementation of synthetic schemes that mirror established methods for accessing the mimicked oligosaccharides. NMR and computational investigations confirm that replacing mannopyranoside units in HMOs with the sp^2-iminosugar analog motif OMJ maintains the available conformational space in aqueous solution. Moreover, the OMJ-capped HMO hemimimetics studied in this work exhibit binding to the mannose-specific lectins ConA, DC-SIGN, and langerin, adopting essentially the same bound conformation as the emulated HMO. Interestingly, the OMJMan glycotope, a mannobiose-like structure, behaves as a heterodivalent ligand for all three lectins, similar to Man_2. Notably, the behavior of the pseudopentasaccharide $(OMJ\text{-}Man)_2Man$ can be rationalized as a divalent OMJMan entity, analogous to Man_5 as a divalent mannobiose derivative. Furthermore, OMJMan clusters benefit from classical multivalent effects, leading to additional enhancements in binding affinity, highlighting their functional biomimetic character. The results also stress that the subtle structural differences between Man and OMJ units can result in distinct preferences for accommodation in the carbohydrate recognition domain (CRD) of specific lectins, especially when presented in multiple copies. Most importantly, it is shown that the selectivity towards the biomedically relevant CLRs DC-SIGN and langerin can be biased with the OMJMan glycotope surrogate. Our findings demonstrate that the overall architecture of the (pseudo)glycocluster, not just the valency, plays a crucial role in this context. We envision that the chemical mimicry strategy can be expanded to access hemimimetics of virtually any natural oligosaccharide containing α-linked monosaccharide residues, thereby opening up new avenues to intervene in carbohydrate-mediated recognition processes.

Experimental Section

General Methods: All commercial chemicals were of reagent grade and were used without further purification. Optical rotations were measured at 20 ± 2 °C in 1-dm tubes on a Jasco P-2000 polarimeter. ^1H (and ^{13}C NMR) spectra were recorded at 500 (125.7) MHz with Bruker 500 DRX o BrukerAvance III spectrometers and chemical shifts (δ) were reported in parts per million (ppm). 1D TOCSY, 2D COSY, HMQC and HSQC experiments were used to assist on NMR assignments. Thin-layer chromatography (TLC) was carried out on aluminum sheets coated with silica gel 60 F_{254} Merck with visualization by UV light and by charring with ethanolic 10% H_2SO_4 and 0.1% ninhydrin. Column chromatography was carried out on Silica Gel 60. ESI mass spectra were recorded on a Bruker Daltonics Esquire6000™ ion-trap mass spectrometer. Elemental analyses were carried out at the Instituto de Investigaciones Químicas (Sevilla, Spain).

The compounds 2-azidoethyl *O*-(α-D-mannopyranosyl)-(1→2)-α-D-mannopyranoside (Man_2, **1**),[24] 2-azidoethyl α-d-mannopyranosyl-(1→2)-α-D-5 *N*,6*O*-oxomethylidenemannonojirimycin (ManOMJ, **2**), 2-azidoethyl α-D-5 *N*,6*O*-oxomethylidenenojirimycinyl-(1→2)-α-D-mannopyranoside (OMJMan, **3**,) 2-azidoethyl α-d-5 *N*,6*O*-oxomethylidenemannonojirimycinyl-(1→2)-α-D-5 *N*,6*O*-oxomethylidenemannonojirimycin (OMJOMJ, **4**), 2-azidoethyl 3,6-di-*O*-α-D-mannopyranosyl-α-D-mannopyranoside (Man_3, **8**),[25] 2-azidoethyl 2,4-di-*O*-benzoyl-α-D-mannopyranoside (**12**),[22] (1*R*)-2,3,4-tri-*O*-acetyl-1-fluoro-5 *N*,6*O*-oxomethylidene-1-deoxymannojirimycin (**13**),[23] *S*-tolyl-3,4,6-tri-*O*-benzoyl-α-D-mannopyranoside (**15**),[24] heptavalent Man-Man βCD7 derivative (**19**),[14] heptavalent OMJ-Man βCD7 derivative (**20**),[14] tetradecavalent Man-Man βCD7 derivative (**21**),[14] tetradecavalent OMJ-Man βCD7 derivative (**22**),[14] tetrapropargylated RAFT (**37**),[43] tetrapropargylated polylisine dendron (**38**),[43] hexapropargylated cyclotriphosphazene (**39**),[44] RAFT-N_3 (**42**),[45] polylysine scaffold-N_3 (**45**),[46] 2,3,4,6-tetra-*O*-benzoyl-α-D-mannopyranosyl trichloroacetimidate (**48**; Supporting information, p S8)[49] and 2-*O*-(2,3,4,6-tetra-*O*-benzoyl-α-D-mannopyranosyl-2,3,4-tri-*O*-benzoyl-α-D-mannopyranosyl trichloroacetimidate (**50**; Supporting information, p S13) were prepared according to described procedures.

Supporting Information

Experimental protocols for all glycosylation, protection/deprotection and multi-CuAAC reactions, compound characterization for all substrates and products, NMR spectra for substrates and products, HPLC chromatograms, detailed protocols for conformational and lectin binding studies by computational and spectroscopic techniques, ELLA, and SPR, including molecular representations, data plots and sensorgrams. The authors have cited additional references within the Supporting Information.[51–64]

Acknowledgements

The authors thank AEI/10.13039/501100011033 (PID2019-105858RB-I00, to C.O.M.), AEI/10.13039/501100011033 and "ERDF A way of making Europe" (PID2020-118403GB-I00, PID2021-125094NB-I00, PID2021-124247OB-C21 and PID2022-141034OB-C21), the COST action GLYCONanoPROBES (CM18132), the Junta de Andalucía (US-1380698 and P20_

Research Article
doi.org/10.1002/chem.202303041
Chemistry Europe
European Chemical Societies Publishing

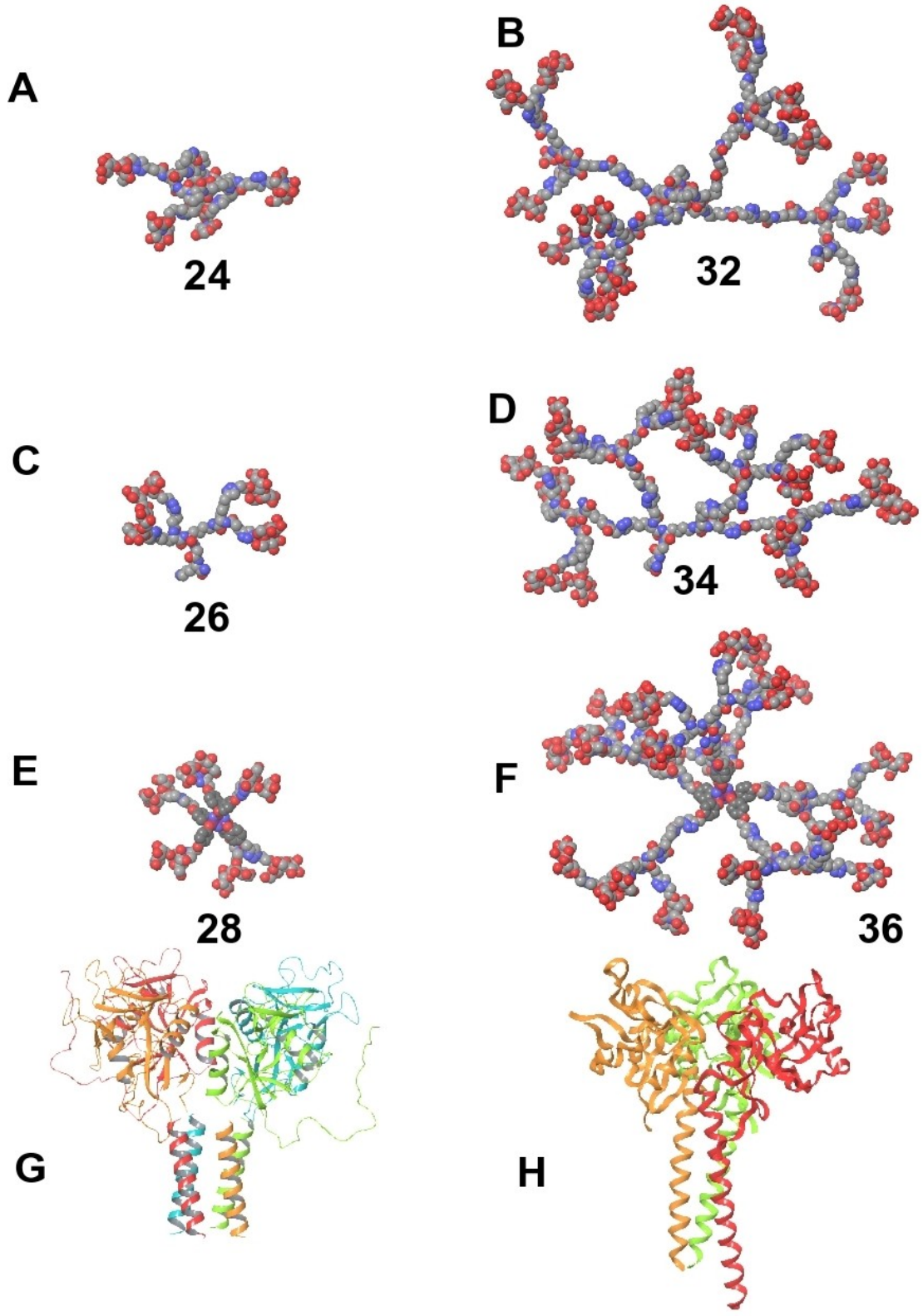

Figure 17. A–F) Representative molecular models of compounds **24, 26, 28, 32, 34**, and **36**. G) Structure of DC-SIGN. H) Structure of langerin. Protein structures are taken from the PDB entries 1k9i and 3PQG with minor automatic modifications, while the ligands are represented as sticks.

00515), and the CITIUS (Univ. Seville), for technical support. J.M.G.F. acknowledges funding by the European Union's Horizon Europe research and innovation programme under the Marie Skłodowska-Curie grant agreement 101130235 – Bicyclos. E I. H.-G. was an FPU fellow (Grant FPU17/03147). M.G.-C. was supported by a postdoctoral fellowship (Contrato de Acceso al

Sistema Español de Ciencia y Tecnologia) funded by the University of Seville This work used the platforms of the Grenoble Instruct-ERIC centre (ISBG; UMS 3518 CNRS-CEAUGA-EMBL) within the Grenoble Partnership for Structural Biology (PSB), supported by FRISBI (ANR-10-INBS-05-02) and GRAL, within the University Grenoble Alpes Graduate School CBH-EUR-GS (ANR-17-URE0003) and the Biomolecular Interaction Platform from cicCartuja (Sevilla). F. F. and O. R. acknowledge the French Agence Nationale de la Recherche PIA for Glyco@Alps (ANR-15-IDEX-02) and together with E.L., for her support, the ANR PRCI LectArray 19-CE18-0019-01. O.R. acknowledges the European Research Council Consolidator Grant "LEGO" (647938).

Conflict of Interests

The authors declare no conflict of interest.

Keywords: carbohydrates · glycomimetics · high-mannose oligosaccharides · lectins · multivalency

[1] a) G. D. Brown, J. A. Willment, L. Whitehead, *Nat. Rev. Immunol.* **2018**, *18*, 374–389; b) S. Mayer, M. -K Raulf, B. Lepenies, *Histochem. Cell Biol.* **2017**, *147*, 223–237.

[2] a) R. Hatinguais, J. A. Willment, G. D. Brown, *Parasite Immunol.* **2023**, *45*, e12951; b) M. E. Mnich, R. van Dalen, N. M. van Sorge, *Front. Cell. Infect. Microbiol.* **2020**, *11*, 134; c) S. Busold, N. A. Nagy, S. W. Tas, R. van Ree, E. C. de Jong, T. B. H. Geijtenbeek, *Front. Immunol.* **2020**, *9*, 2754; d) M. S. Pereira, I. Alves, M. Vicente, A. Campar, M. C. Silva, N. A. Padrão, V. Pinto, Â. Fernandes, A. M. Dias, S. S. Pinho, *Front. Immunol.* **2018**, *9*, 2754; e) J. T. Monteiro, B. Lepenies, *Viruses* **2017**, *9*, 59.

[3] a) P. Valverde, J. D. Martínez, F. J. Cañada, A. Ardá, J. Jiménez-Barbero, *ChemBioChem* **2020**, *21*, 2999–3025; b) J. Cramer, *RSC Med. Chem.* **2021**, *12*, 1985–2000.

[4] a) M. Nagae, Y. Yamaguchi, *Curr. Top. Microbiol. Immunol.* **2020**, *429*, 147–176; b) H. Moriuchi, H. Unno, S. Goda, H. Tateno, J. Hirabayashi, T. Hatakeyama, *Biochim. Biophys. Acta* **2015**, *1850*, 1457–1465.

[5] a) D. S. Kwon, G. Gregorio, N. Bitton, W. A. Hendrickson, D. R. Littman, *Immunity* **2002**, *16*, 135–144; b) T. B. Geijtenbeek, D. S. Kwon, R. Torensma, S. J. van Vliet, G. C. van Duijnhoven, J. Middel, I. L. Cornelissen, H. S. Nottet, V. N. KewalRamani, D. R. Littman, C. G. Figdor, Y. van Kooyk, *Cell* **2000**, *100*, 587–597.

[6] L. de Witte, A. Nabatov, M. Pion, D. Fluitsma, M. A. de Jong, T. de Gruijl, V. Piguet, Y. van Kooyk, T. B. Geijtenbeek, *Nat. Med.* **2007**, *13*, 367–371.

[7] a) J. Rojo, P. Nieto, J. L. de Paz, *Curr. Med. Chem.* **2022**, *29*, 1173–1192, b) R. Wawrzinek, E.-C. Wamhoff, J. Lefebre, M. Rentzsch, G, Bachem, G. Domeniconi, J. Schulze, F. F. Fuchsberger, H. Zhang, C. Modenutti, L. Schnirch, M. A. Marti, O. Schwardt, M. Bräutigam, M. Guberman, D. Hauck, P. H. Seeberger, O. Seitz, A. Titz, B. Ernst, C. Rademacher, *J. Am. Chem. Soc.* **2021**, *143*, 18977–18988; c) E.-C. Wamhoff, J. Schulze, L. Bellmann, M. Rentzsch, G. Bachem, F. F. Fuchsberger, J. Rademacher, M. Hermann, B. Del Frari, R van Dalen, D. Hartmann, N, M. van Sorge, O. Seitz, P. Stoitzner, C. Rademacher, *ACS Cent. Sci.* **2019**, *5*, 808–820; d) J. C. Muñoz-García, E. Chabrol, R. R. Vives, A. Thomas, J. L. de Paz, J. Rojo, A. Imberty, F. Fieschi, P. M. Nieto, J. Angulo, *J. Am. Chem. Soc.* **2015**, *137*, 4100–4110.

[8] a) E. Shanina, S. Kuhaudomlarp, E. Siebs, F. F. Fuchsberger, M. Denis, P. S. F. C. Gomes, M. H. Clausen, P. H. Seeberger, D. Rognan, A. Titz, A. Imberty, C. Rademacher, *Commun. Chem.* **2022**, *5*, 64; b) J. Schulze, H. Baukmann, R. Wawrzinek, F. F. Fuchsberger, E. Specker, J. Aretz, M. Nazaré, C. Rademacher, *ACS Chem. Biol.* **2018**, *13*, 3229–3235; c) J. Aretz, H. Baukmann, E. Shanina, J. Hanske, R. Wawrzinek, V. A. Zapol'skii, P. H. Seeberger, D. E. Kaufmann, C. Rademacher, *Angew. Chem. Int. Ed.* **2017**, *56*, 7292–7296; d) S. Sattin, A. Daghetti, M. Thépaut, A. Berzi, M. Sánchez-Navarro, G. Tabarani, J. Rojo, F. Fieschi, A. Bernardi, *ACS Chem. Biol.* **2010**, *5*, 301–312; e) M. J. Borrok, L. L. Kiessling, *J. Am. Chem. Soc.* **2007**, *129*, 12780–12785.

[9] a) J. Angulo, I. Díaz, J. J. Reina, G. Tabarani, F. Fieschi, J. Rojo, P. M. Nieto, *ChemBioChem* **2008**, *22*, 2225–22257; b) H. Feinber, R. Castelli, K. Drickamer, P. H. Seeberger, W. I. Weis, *J. Biol. Chem.* **2007**, *282*, 4202–4209.

[10] A. Holla, A. Skerra, *Protein Eng. Des. Sel.* **2011**, *24*, 659–669.

[11] a) D. K. Mandal, N. Kishore, C. F. Brewer, *Biochemistry.* **1994**, *33*, 1149–1156; b) B. A. Williams, M. C. Chervenak, E. J. Toone, *J. Biol. Chem.* **1992**, *267*, 22907–22911; c) D. N. Moothoo, B. Canan, R. A. Field, J. H. Naismith, *Glycobiology* **1999**, *9*, 539–545.

[12] P. Rohse, S. Weickert, M. Drescher, V. Wittmann, *Chem. Sci.* **2020**, *11*, 5227–5237.

[13] a) M. Mammen, S.-K. Choi, G. M. Whitesides, *Angew. Chem. Int. Ed.* **1998**, *37*, 2755–2794; b) C. R. Bertozzi, L. L. Kiessling, *Science* **2001**, *291*, 2357–2364; c) L. L. Kiessling, J. E. Gestwicki, L. E. Strong, *Angew. Chem. Int. Ed.* **2006**, *45*, 2348–2368; d) S. Cecioni, A. Imberty, S. Vidal, *Chem. Rev.* **2015**, *115*, 525–561; e) M. Martínez-Bailén, J. Rojo, J. Ramos-Soriano, *Chem. Soc. Rev.* **2023**, *52*, 536–572.

[14] I. Herrera-González, M. Thépaut, E. M. Sánchez-Fernández, A. di Maio, C. Vivès, J. Rojo, J. M. García Fernández, F. Fieschi, P. M. Nieto, C. Ortiz Mellet, *Chem. Commun.* **2022**, *58*, 12086–12089.

[15] a) J. L. Jiménez Blanco, V. Díaz Pérez, C. Ortiz Mellet, J. Fuentes, J. M. García Fernández, J. C. Díaz Arribas, F. J. Cañada, *Chem. Commun.* **1997**, 1969–1970; b) M. I. García-Moreno, J. M. Benito, C. Ortiz Mellet, J. M. García Fernández, *J. Org. Chem.* **2001**, *66*, 7604–7614; c) Z. Luan, K. Higaki, M. Aguilar-Moncayo, L. Li, H. Ninomiya, E. Nanba, K. Ohno, M. I. García-Moreno, C. Ortiz Mellet, J. M. García Fernández, Y. Suzuki, *ChemBioChem* **2010**, *11*, 2453–2464; d) M. I. García-Moreno, P. Díaz-Pérez, C. Ortiz Mellet, J. M. García Fernández, *J. Org. Chem.* **2003**, *68*, 8890–8901; e) M. Aguilar-Moncayo, M. I. García-Moreno, A. Trapero, M. Egido-Gabás, A. Llebaria, J. M. García Fernández, C. Ortiz Mellet, *Org. Biomol. Chem.* **2011**, *9*, 3698–3713; f) T. Mena-Barragán, A. Narita, D. Matias, G. Tiscornia, E. Nanba, K. Ohno, Y. Suzuki, K. Higaki, J. M. Garcia Fernández, C. Ortiz Mellet, *Angew. Chem. Int. Ed.* **2015**, *54*, 11696–11700; g) M. González-Cuesta, I. Herrera-González, M. I. García-Moreno, R. A. Ashmus, D. J. Vocadlo, J. M. García Fernández, E. Nanba, K. Higaki, C. Ortiz Mellet, *J. Enzyme Inhib. Med. Chem.* **2022**, *37*, 1364–1374; h) M. González-Cuesta, P. Sidhu, R. A. Ashmus, A. Males, C. Proceviat, Z. Madden, J. C. Rogalski, J. A. Busmann, L. J. Foster, J. M. García Fernández, G. J. Davies, C. Ortiz Mellet, D. J. Vocadlo, *J. Am. Chem. Soc.* **2022**, *144*, 832–844.

[16] a) M. C. Padilla-Pérez, E. M. Sánchez-Fernández, A. González-Bakker, A. Puerta, J. M. Padrón, F. Martín-Loro, A. I. Arroba, J. M. García Fernández, C. Ortiz Mellet, *Eur. J. Med. Chem.* **2023**, 115390; b) M. Gonzalez-Cuesta, A. C.-Y. Lai, P.-Y. Chi, I.-L. Hsu, N.-T. Liu, K.-C. Wu, J. M. Garcia Fernandez, Y.-J. Chang, C. Ortiz Mellet, *J. Med. Chem.* **2023**, *66*, 4768–4783; c) I. A. Bermejo, C. D. Navo, J. Castro-López, A. Guerreiro, E. Jiménez-Moreno, E. M. Sánchez-Fernández, F. García-Martín, H. Hinou, S.-I. Nishimura, J. M. García Fernández, C. Ortiz Mellet, A. Avenoza, J. H. Busto, G. J. L. Bernardes, R. Hurtado-Guerrero, J. M. Peregrina, F. Corzana, *Chem. Sci.* **2020**, *11*, 3996–4006; d) P. A. Guillen-Poza, E. M. Sánchez-Fernández, G. Artigas, J. M. García Fernández, H. Hinou, C. Ortiz Mellet, S.-I. Nishimura, F. Garcia-Martin, *J. Med. Chem.* **2020**, *63*, 8524–8533; e) E. M. Sánchez Fernández, C. D. Navo, N. Martínez-Sáez, R. Gonçalves-Pereira, V. J. Somovilla, A. Avenoza, J. H. Busto, G. J. L. Bernardes, G. Jiménez-Osés, F. Corzana, J. M. García Fernández, C. Ortiz Mellet, J. M. Peregrina, *Org. Lett.* **2016**, *18*, 3890–3893; f) G. Allan, H. Ouadid-Ahidouch, E. M. Sánchez-Fernández, R. Rísquez-Cuadro, J. M. García Fernández, C. Ortiz Mellet, A. Ahidouch, *PLoS ONE* **2013**, *8*, e76411; g) E. M. Sánchez-Fernández, R. Rísquez-Cuadro, C. Ortiz Mellet, J. M. García Fernández, P. M. Nieto-Mesa, J. Angulo-Álvarez, *Chem. Eur. J.* **2012**, *18*, 8527–8539; h) E. M. Sánchez-Fernández, R. Rísquez-Cuadro, M. Chasseraud, A. Ahidouch, C. Ortiz Mellet, H. Ouadid-Ahidouch, J. M. García Fernández, *Chem. Commun.* **2010**, *46*, 5328.

[17] P. Díaz Pérez, M. I. García-Moreno, C. Ortiz Mellet, J. M. García Fernández, *Eur. J. Org. Chem.* **2005**, 2903–2913; R. Rísquez-Cuadro, R. Matsumoto, F. Ortega-Caballero, E. Nanba, K. Higaki, J. M. García Fernández, C. Ortiz Mellet, *J. Med. Chem.* **2019**, *62*, 5832–5843.

[18] a) Á. Martínez, C. Ortiz Mellet, J. M. García Fernández, *Chem. Soc. Rev.* **2013**, *42*, 4746–4773; b) G. Rivero-Barbarroja, J. M. Benito, C. Ortiz Mellet, J. M. García Fernández, *Nanomaterials* **2020**, *10*, 2517.

[19] a) J. J. Reina, S. Sattin, D. Invernizzi, S. Mari, L. Martínez-Prats, G. Tabarani, F. Fieschi, R. Delgado, P. M. Nieto, J. Rojo, A. Bernardi, *ChemMedChem* **2007**, *2*, 1030–1036; b) M. Thépaut, C. Guzzi, I. Sutkeviciute, S. Sattin, R. Ribeiro-Viana, N. Varga, E. Chabrol, J. Rojo, A. Bernardi, J. Angulo, P. M. Nieto, F. Fieschi, *J. Am. Chem. Soc.* **2013**, *135*, 2518–2529; c) S. Ordanini, N. Varga, V. Porkolab, M. Thépaut, L. Belvisi,

A. Bertaglia, A. Palmioli, A. Berzi, D. Trabattoni, M. Clerici, F. Fieschi, A. Bernardi, *Chem. Commun.* **2015**, *51*, 3816–3819; d) V. Porkolab, E. Chabrol, N. Varga, S. Ordanini, I. Sutkeviciute, M. Thépaut, M. J. García-Jiménez, E. Girard, P. M. Nieto, A. Bernardi, F. Fieschi, *ACS Chem. Biol.* **2018**, *13*, 600–608; e) L. Medve, S. Achilli, J. Guzman-Caldentey, M. Thépaut, L. Senaldi, A. Le Roy, S. Sattin, C. Ebel, C. Vivès, S. Martin-Santamaria, A. Bernardi, F. Fieschi, *Chem. Eur. J.* **2019**, *25*, 14659–14668; f) S. Pollastri, C. Delaunay, M. Thépaut, F. Fieschi, A. Bernardi, *Chem. Commun.* **2022**, *58*, 5136–5139; g) G. Goti, C. Colombo, S. Achilli, C. Vives, M. Thepaut, J. Luczkowiak, N. Labiod, R. Delgado, F. Fieschi, A. Bernardi, *Eur. J. Org. Chem.* **2022**, e202200113; h) V. Porkolab, M. Lepsík, S. Ordanini, A. St John, A. Le Roy, M. Thépaut, E. Paci, C. Ebel, A. Bernardi, F. Fieschi, *ACS Cent. Sci.* **2023**, **9**, 709–718.

[20] a) V. Cendret, M. François-Heude, A. Méndez-Ardoy, V. Moreau, J. M. García Fernández, F. Djedaïni-Pilard, *Chem. Commun.* **2012**, *48*, 3733–3735; b) M. François-Heude, A. Méndez-Ardoy, V. Cendret, P. Lafite, R. Daniellou, C. Ortiz Mellet, J. M. García Fernández, V. Moreau, F. Djedaïni-Pilard, *Chem. Eur. J.* **2015**, *21*, 1978–1991; c) J. Cramer, A. Lakkaichi, B. Aliu, R. P. Jakob, S. Klein, I. Cattaneo, X. Jiang, S. Rabbani, O. Schwardt, G. Zimmer, M. Ciancaglini, T. A. Mota, T. Maier, B. Ernst, *J. Am. Chem. Soc.* **2021**, *143*, 17465–17478.

[21] a) M. Gómez-García, J. M. Benito, D. Rodríguez-Lucena, J. Yu, K. Chmurski, C. Ortiz Mellet, R. Gutiérrez Gallego, A. Maestre, J. Defaye, J. M. García Fernández, *J. Am. Chem. Soc.* **2005**, *127*, 7970–7971; b) M. Gómez-García, J. M. Benito, R. Gutierrez-Gallego, A. Maestre, C. Ortiz Mellet, J. M. García Fernández, J. L. Jiménez Blanco, *Org. Biomol. Chem.* **2010**, *8*, 1849–1860; c) M. Gómez-García, J. M. Benito, A. P. Butera, C. Ortiz Mellet, J. M. García Fernández, J. L. Jiménez Blanco, *J. Org. Chem.* **2012**, *77*, 1273–1288; d) J. L. Jiménez Blanco, C. Ortiz Mellet, J. M. García Fernández, *Chem. Soc. Rev.* **2013**, *42*, 4518; e) D. Ponader, P. Maffre, J. Aretz, D. Pussak, N. M. Ninnemann, S. Schmidt, P. H. Seeberger, C. Rademacher, G. U. Nienhaus, L. Hartmann, *J. Am. Chem. Soc.* **2014**, *136*, 2008–2016; f) C. Ortiz Mellet, J.-F. Nierengarten, J. M. García Fernández, *J. Mater. Chem. B* **2017**, *5*, 6428–6436; g) K. S. Bücher, P. B. Konietzny, N. L. Snyder, L. Hartmann, *Chem. Eur. J.* **2019**, *25*, 3301–3309; h) M. González-Cuesta, C. Ortiz Mellet, J. M. García Fernández, *Chem. Commun.* **2020**, *56*, 5207–5222; i) S. O. Jaeschke, I. vom Sondern, T. K. Lindhorst, *Org. Biomol. Chem.* **2021**, *19*, 7013–7023; j) M. Liu, L. Z. X. Huang, A. A. Smits, C. Büll, Y. Narimatsu, F. J. M. van Kuppeveld, H. Clausen, C. A. M. de Haan, E. de Vries, *Nat. Commun.* **2022**, *13*, 4054.

[22] M. Dowlut, D. G. Hall, O. Hindsgaul, *J. Org. Chem.* **2005**, *70*, 9809–9813.

[23] E. M. Sánchez-Fernández, R. Gonçalves-Pereira, R. Rísquez-Cuadro, G. B. Plata, J. M. Padrón, J. M. García Fernández, C. Ortiz Mellet, *Carbohydr. Res.* **2016**, *429*, 113–122.

[24] J. J. Reina, A. Di Maio, J. Ramos-Soriano, R. C. Figueiredo, J. Rojo, *Org. Biomol. Chem.* **2016**, *14*, 2873–2882.

[25] T. K. Lindhorst, K. Bruegge, A. Fuchs, O. Sperling, *Beilstein J. Org. Chem.* **2010**, *6*, 801–809.

[26] X. Li, S. Cheng, Y. Wang, L. Ma, Y. Shao, Y. Double-target anti-HIV (anti-human immunodeficiency virus) glycopeptide compound and application thereof. Patent No. CN105273064, China, **2016**.

[27] M. Lipton, W. C. Still, *J. Comput. Chem.* **1988**, *9*, 343–355.

[28] T. Peters, B. Meyer, R. Stuike-Prill, R. Somorjai, J. R. Brisson, *Carbohydr. Res.* **1993**, *238*, 49–73.

[29] F. Guarnieri, W. C. Still, *J. Comput. Chem.* **1994**, *15*, 1302–1310.

[30] Schrödinger Release 2019: Maestro, Schrödinger, LLC, New York, NY, **2019**.

[31] A. Bernardi, A. Colombo, I. Sánchez-Medina, *Carbohydr. Res.* **2004**, *339*, 967–973.

[32] R. J. Woods, A. Pathiaseril, M. R. Wormald, C. J. Edge, R. A. Dwek, *Eur. J. Biochem.* **1998**, *259*, 372–386.

[33] a) O. H. Hashim, J. J. Jayapalan, C. Lee, *PeerJ* **2017**, *5*, e3784; b) A. M. Wu, J. H. Liu, *Glycoconjugate J.* **2019**, *36*, 175–183.

[34] a) J. J. Lundquist, E. J. Toone, *Chem. Rev.* **2002**, *102*, 555–578; b) S. G. Gouin, J. M. García Fernández, E. Vanquelef, F.-Y. Dupradeau, E. Salomonsson, H. Leffler, M. Ortega-Muñoz, U. J. Nilsson, J. Kovensky, *ChemBioChem* **2010**, *11*, 1430–1442.

[35] I. J. Goldstein, C. M. Reichert, A. Misaki, *Ann. N. Y. Acad. Sci.* **1974**, *234*, 283–296.

[36] P. Krishnan, A. Singla, C.-A. Lee, J. D. Weatherston, N. C. Worstell, H.-J. Wu, *Colloids Surf. B: Biointerfaces* **2017**, *160*, 281–288.

[37] Y. Ohyama, K. Kasai, H. Nomoto, Y. Inoue, *J. Biol. Chem.* **1985**, *260*, 6882–6887.

[38] D. N. Moothoo, J. H. Naismith, *Glycobiology* **1998**, *8*, 173–181.

[39] a) N. Obermajer, S. Sattin, C. Colombo, M. Bruno, U. Svajger, M. Anderluh, A. Bernardi, *Mol. Divers.* **2011**, *15*, 347–360; b) J. D. Martínez, A. Infantino, P. Valverde, T. Diercks, S. Delgado, N. C. Reichardt, A. Ardá, F. J. Cañada, S. Oscarson, J. Jiménez-Barbero, *Pharmaceuticals* **2020**, *13*, 179.

[40] H. Feinberg, D. A. Mitchell, K. Drickamer, W. I. Weis, *Science* **2001**, *294*, 2163–2166.

[41] Y. Guo, H. Feinberg, E. Conroy, D. A. Mitchell, R. Alvarez, O. Blixt, M. E. Taylor, W. I. Weis, K. Drickamer, *Nat. Struct. Mol. Biol.* **2004**, *11*, 591–598.

[42] H. Feinberg, M. E. Taylor, N. Razi, R. McBride, Y. A. Knirel, S. A. Graham, K. Drickamer, W. I. Weis, *J. Mol. Biol.* **2011**, *405*, 1027–1039.

[43] M. Hovorková, J. Červený, L. Bumba, H. Pelantová, J. Cvačka, V. Křen, O. Renaudet, D. Goyard, P. Bojarová, *Bioorg. Chem.* **2022**, *131*, 106279.

[44] L. Abbassi, Y. M. Chabre, K. Nottari, A. A. Arnold, S. André, J. Josserand, H.-J. Gabius, R. Roy, *Polym. Chem.* **2015**, *6*, 7666–7683.

[45] I. Bossu, N. Berthet, P. Dumy, O. Renaudet, *J. Carbohydr. Chem.* **2011**, *30*, 458–468.

[46] C. Pifferi, D. Goyard, E. Gillon, A. Imberty, O. Renaudet, *ChemPlusChem* **2017**, *82*, 390–398.

[47] I. Baussanne, J. M. Benito, C. Ortiz Mellet, J. M. García Fernández, J. Defaye, *ChemBioChem* **2001**, *2*, 777–783.

[48] V. Porkolab, C. Pifferi, I. Sutkeviciute, S. Ordanini, M. Taouai, M. Thépaut, C. Vivès, M. Benazza, A. Bernardi, O. Renaudet, F. Fieschi, *Org. Biomol. Chem.* **2020**, *18*, 4763–4772.

[49] D. Lee, J. R. Kowalczyk, V. J. Muir, P. M. Rendle, M. A. Brimble, *Carbohydr. Res.* **2007**, *342*, 2628–2634.

[50] J. Ramos-Soriano, M. C. de la Fuente, N. de la Cruz, R. C. Figueiredo, J. Rojo, J. J. Reina, *Org Biomol Chem.* **2017**, *15*, 8877–8882.

[51] M. J. Thrippleton, J. Keeler, *Angew. Chem. Int. Ed.* **2003**, *42*, 3938–3941.

[52] K. Stott, J. Keeler, Q. N. Van, A. J. Shaka, *J. Magn. Reson.* **1997**, *125*, 302–324.

[53] B. Meyer, T. Peters, *Angew. Chem. Int. Ed.* **2003**, *42*, 864–890.

[54] J. Angulo, P. M. Nieto, *Eur. Biophys. J.* **2011**, *40*, 1357–1369.

[55] M. J. García-Jiménez, S. Gil-Caballero, S. Maza, F. Corzana, F. Juárez-Vicente, J. R. Miles, K. Sakamoto, K. Kadomatsu, M. García-Domínguez, J. L. Paz, P. M. Nieto, *Chem Eur. J.* **2021**, *27*, 12395–12409.

[56] H. Hu, K. Krishnamurthy, *J. Magn. Reson.* **2006**, *182*, 173–177.

[57] W. C. Still, A. Tempczyk, R. C. Hawley, T. Hendrickson, *J. Am.Chem. Soc.* **1990**, *112*, 6127–6129.

[58] J. M. Goodman, W. C. Still, *J. Comput. Chem.* **1991**, *12*, 1110–1117.

[59] O. Trott, A. J. Olson, *J. Comput. Chem.* **2010**, *31*, 455–461.

[60] G. M. Sastry, M. Adzhigirey, T. Day, R. Annabhimoju, W. Sherman, *J. Comput. Aided Mol. Des.* **2013**, *27*, 221–234.

[61] G. Tabarani, M. Thépaut, D. Stroebel, C. Ebel, C. Vivès, P. Vachette, D. Durand, F. Fieschi, *J. Biol. Chem.* **2009**, *284*, 21229–21240.

[62] S. Achilli, J. T. Monteiro, S. Serna, S. Mayer-Lambertz, M. Thépaut, A. Le Roy, C. Ebel, N.-C. Reichardt, B. Lepenies, F. Fieschi, C. Vivès, *Int. J. Mol. Sci.* **2020**, *21*, 5290.

[63] F. Halary, A. Amara, H. Lortat-Jacob, M. Messerle, T. Delaunay, C. Houlès, F. Fieschi, F. Arenzana-Seisdedos, J.-F. Moreau, J. Déchanet-Merville, *Immunity* **2002**, *17*, 653–664.

[64] M. Andreini, D. Doknic, I. Sutkeviciute, J. J. Reina, J. Duan, E. Chabrol, M. Thepaut, E. Moroni, F. Doro, L. Belvisi, J. Weiser, J. Rojo, F. Fieschi, A. Bernardi, *Org. Biomol. Chem.* **2011**, *9*, 5778–5786.

Manuscript received: September 18, 2023
Accepted manuscript online: October 12, 2023
Version of record online: ■■, ■■

RESEARCH ARTICLE

The "carbohydrate chemical mimicry" of sp^2-iminosugars enables the synthesis of high-mannose-type oligosaccharide analogs whose solution and lectin bound conformations match those of the natural partners. Upon multivalent presentation, enhanced affinities towards ConA, DC-SIGN and langerin are achieved, with distinct selectivity profiles.

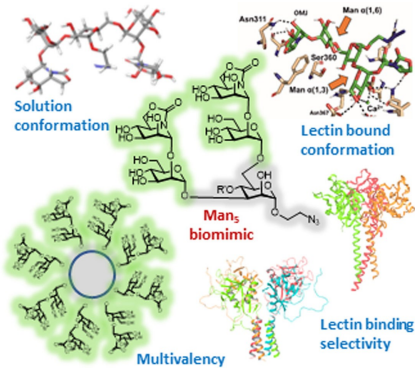

Dr. I. Herrera-González, Dr. M. González-Cuesta, Dr. M. Thépaut, Dr. E. Laigre, Dr. D. Goyard, Dr. J. Rojo, Dr. J. M. García Fernández, Prof. F. Fieschi, Prof. O. Renaudet, Dr. P. M. Nieto, Prof. C. Ortiz Mellet**

1 – 22

High-Mannose Oligosaccharide Hemimimetics that Recapitulate the Conformation and Binding Mode to Concanavalin A, DC-SIGN and Langerin